Polarons, vacancies, vacancy associations, and defect states in multiferroic BiFeO 3

Grégory Geneste, Charles Paillard, Brahim Dkhil

Polarons, vacancies, vacancy associations, and defect states in multiferroic $BiFeO_3$

Grégory Geneste,[1,*] Charles Paillard,[2,3] and Brahim Dkhil[2]
[1]*CEA, DAM, DIF, F-91297 Arpajon, France*
[2]*Laboratoire Structures, Propriétés et Modélisation des Solides, UMR CNRS 8580, CentraleSupélec, Université Paris-Saclay, 91190 Gif-sur-Yvette, France*
[3]*Physics Department, University of Arkansas, 825 W. Dickson St., Fayetteville, Arkansas 72701, USA*

(Received 5 June 2018; revised manuscript received 2 October 2018; published 9 January 2019)

Oxygen, bismuth, and iron vacancies are studied by density-functional theory calculations in multiferroic bismuth ferrite in oxidative and reducing external conditions. We accurately describe the localized electronic states associated with isolated defects. Oxygen-rich conditions provide fully ionized oxygen vacancies, and ionized or partially ionized cationic vacancies, possibly yielding *p*-type conductivity mediated by oxygen-type holes. Oxygen-poor conditions provide fully ionized vacancies and a much smaller concentration of electronic carriers. Cationic and oxygen vacancies tend to pair (Bi-O, Fe-O) with an associated electric dipole being as close as possible to the polar axis, possibly leading to imprint effects. This clustering also results in an extended stability domain for the ionized defects. Furthermore, O and Fe vacancies are respectively associated with Fe-3*d* and O-2*p* type moderately deep defect states spatially localized close to the defect. The charge-neutral Fe vacancy possesses an electric dipole, despite being a point defect. Bi vacancies may be found in several metastable electronic states, with in the most stable one, a mid-gap band of defect states with Fe-3*d* character, in addition to the three O-2*p* defect states associated to the acceptor nature of this defect. Finally, electrons released in the lattice by oxygen vacancies, if not captured by acceptor defects, tend to localize as small polarons, while holes released by cationic vacancies, if not captured by donor defects, are associated with delocalized Bloch-like band states.

DOI: 10.1103/PhysRevB.99.024104

I. INTRODUCTION

Bismuth ferrite is the model multiferroic compound. It concurrently exhibits ferroelectricity (with large polarization) and a complex antiferromagnetic cycloidal magnetic order, both of which survive well beyond room temperature [1]. As a result, $BiFeO_3$ (BFO) has been considered as the test model to understand the physics behind multiferroic couplings and develop functional properties such as piezoelectricity and magnetoelectricity. In addition, the rather small band gap (∼2.5–2.8 eV [2–6]) compared to classical ferroelectric perovskite oxides, has made BFO the prominent system to study photoinduced phenomena in ferroelectrics, such as photovoltaics and photostriction [7,8].

Despite the natural richness of BFO, it remains a material difficult to work with, in particular owing to its tendency to exhibit strong leakage currents [9–13]. The origin of those leakage currents, detrimental to the ferroelectric properties, has often been blamed on the presence of oxygen vacancies [14–17], although Bi vacancies, causing *p* doping, are also likely to play a role [18,19]. Evidences of the presence of oxygen vacancies, which induce states roughly 0.3–0.5 eV below the conduction band minimum, have been gathered recently using optical techniques such as optical absorption, cathodoluminescence or photoconductivity [20,21].

In ferroelectric (FE) materials, point defects are also believed to be strongly related to imprint (preferential direction of the polarization due to dipolar defects), as is the case, e.g., for hydrogen interstitials [22,23] or oxygen vacancies at surfaces [24,25]. Note that in the limit case scenario of a large concentration of neutral oxygen vacancies, the polarization can even disappear [26,27]. Moreover, point and bidefects have been shown to preferentially form at ferroelectric domain walls [28–30], and thus pin them, which impacts piezoelectric and switching properties, for which domain wall motion is often key. Some defects can thus provide the necessary free carriers to stabilize charged domain walls, which may help in the design of a new kind of reconfigurable electronic nanocircuits. Interestingly, they may also provide intragap absorption centers, which may improve the absorption properties and solar power conversion efficiency of ferroelectric-based solar cells.

No matter whether the effects of point defects on the properties of interest in FE systems are beneficial or detrimental, defects are unavoidable byproducts of the synthesis of any material. Their concentration depends largely on the fabrication process, which is why understanding the thermodynamics of their formation is critically important in order to control their number, location ("defect engineering," doping [31]), and the resulting impact on the ferroic properties [32,33].

First-principles density-functional calculations are currently used today to model the properties of single point defects, either neutral or charged, allowing to compute their formation energies. Although these energies make sense only in the dilute limit, supercells of moderate size, compatible with *ab initio* techniques, can be used, provided a set of post-treatments and corrections are applied to the results [34]. However, the interactions between point defects, especially in

*gregory.geneste@cea.fr

FE materials, have been less investigated. Yet, charged defects are present in crystals simultaneously to other—charge compensating—defects, sometimes by pairs of interacting defects [35]. The two most popular associations of defects in ionic crystals are the Frenkel pair (vacancy + interstitial) and the Schottky defect (presence of vacancies corresponding to the removal of a formula unit). The association of two opposite charged defects is of particular interest in a ferroelectric compound because such an entity carries an electric dipole, which is likely to couple to the polarization, possibly creating an imprint effect.

In BFO, a number of previous *ab initio* studies have investigated the formation of vacancies and antisite defects [18,19,36–40]. Paudel *et al* [18] showed, from LDA+U calculations, that in oxygen-rich conditions, cationic vacancies may form rather easily. They predicted, for these defects, moderate transition energy levels, typically up to ∼0.5 eV, indicating that they can be ionized and liberate holes, producing p-type conductivity. In oxygen-poor conditions, cationic vacancies are fully ionized. Charge compensation is, in both cases, ensured by ionized oxygen vacancies V_O^{2+}. Shimada *et al.* [40] from hybrid HSE06 calculations, arrived at similar conclusions, with the exception that Bi vacancies are described as rather shallow defects.

In this work, we study, by density-functional theory calculations, the Bi, Fe, and O monovacancies, and the Bi-O and Fe-O divacancies in BFO, in different possible relative atomic configurations. We show how these two bidefects can cause an imprint effect on the polarization. We compute the formation and association energies of the defects. The three single vacancies generate localized states within the band gap, with a particular complexity in the case of the Bi vacancy. We also show that the Fe vacancy alone carries an electric dipole. We finally examine whether the released electronic charges (electrons or holes) may localize or not as self-trapped small polarons.

II. COMPUTATIONAL DETAILS

A. Electronic structure of $BiFeO_3$

BFO is an insulating ferroelectric and antiferromagnetic (G-type) oxide, with Fe ions in oxidation state +3, in a high-spin configuration ($3d^5_\uparrow$, $3d^0_\downarrow$) (with the occupied spin channel alternating from an ion to the next one). A weak ferromagnetism related to a slight spin canting is also observed (but will not be considered in the present work). The bottom of the conduction band (CB) in BFO is formed by the empty Fe $3d$ states. The occupied Fe $3d$ states are stabilized by electronic interactions and fall in the valence band (VB), where they mix with oxygen $2p$ states. In the high-spin half-filled electronic configuration of the Fe^{3+} ion, the exchange energy is large. This is why, even when using the standard approximations to the exchange-correlation (XC) energy (LDA, GGA), there is a gap opening between the occupied and empty $3d$ orbitals. This gap is, however, relatively small; in LDA, the Kohn-Sham (KS) band gap is found in the literature between 0.4 and 0.9 eV [41–43]. In GGA, the KS band gap is larger, typically between 0.9 and 1.5 eV [42,44–46].

However, the band gap is in better agreement with the experimental value using LDA+U, with U applied on Fe d orbitals. Several authors [41,42,46] showed that in LDA and GGA, the occupied Fe $3d$ states are rather uniformly distributed over the whole valence band. In LDA, the valence band top is thus a mixture of O $2p$ and Fe $3d$ states, which therefore drives the picture of a mixed Mott/charge-transfer insulator. However, using LDA+U, it was showed that the occupied Fe $3d$ progressively concentrate at the bottom of the valence band [41,42] with increasing U, giving therefore rather for BFO the picture of a charge-transfer insulator, with a band gap of type O $2p$ → Fe $3d$. This fact is also corroborated by hybrid HSE calculations [47]. We reproduce this character in Fig. 1. This localization of the correlated Fe states at the bottom of the valence band in LDA+U is related to the high-spin state of Fe (similar behavior may be observed, for instance, in some cobalt oxides [48–51]).

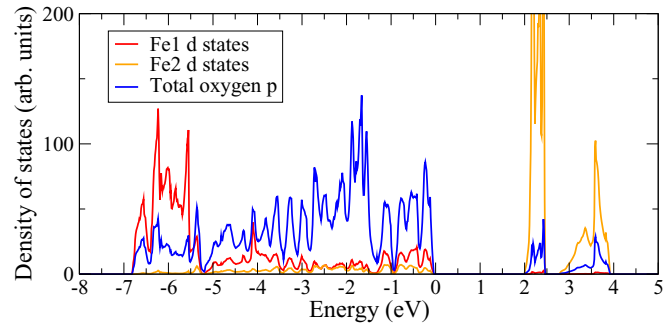

FIG. 1. Electronic density of states of BFO projected on Fe d and O p states, for one of the two spin channels, as obtained by LDA+U ($U = 3.87$ eV on Fe d orbitals). The two Fe atoms are antiferromagnetically coupled. The Fermi energy is set at 0 eV.

B. Density-functional calculations

In this work, we perform first-principles spin-polarized density-functional theory (DFT) calculations [52]. We have used two XC functionals: (i) mainly the LDA+U (Hubbard correction on the Fe $3d$ orbitals, with $U = 3.87$ eV [53] and $J = 0$) and (ii) the GGA-PBE. [54] We use the ABINIT [55] code, in the framework of the projector augmented wave (PAW) method [56,57]. In addition to the Bi $6s$ and $6p$, the Fe $4s$ and $3d$, and the O $2s$ and $2p$ valence électrons, our PAW datasets also include as semicore electrons the Bi $5d$ and Fe $3s$ and $3p$. All the calculations are spin-polarized, with the spin degrees of freedom being accounted for in the framework of collinear magnetism (i.e., the magnetization is a scalar quantity). Thus, spin-orbit coupling is ignored. The defects are simulated using an 80-atom supercell of BFO ($2 \times 2 \times 2$ in terms of the primitive ten-atom rhombohedral unit cell), periodically repeated in the three directions, starting from its ground-state rhombohedral $R3c$ structure with G-type antiferromagnetism. A $2 \times 2 \times 2$ k mesh is used to sample the first Brillouin zone associated with the $2 \times 2 \times 2$ supercell for all the structural optimizations (equivalent to a $4 \times 4 \times 4$ mesh in the primitive ten-atom unit cell). All the structural optimizations using supercells are performed with the supercell vectors maintained fixed according to those of perfect rhombohedral BFO. A plane-wave cutoff of 25 Ha is used. Structural optimizations are performed using the Broyden-Fletcher-Goldfarb-Shanno algorithm and the tolerance criterion is $4 \times$

TABLE I. Lattice constant a, rhombohedral angle α, KS band gap E_g^{KS} and spin magnetic moment on Fe atom (M_{Fe}) obtained after structural relaxation with different functionals.

	LDA	LDA + U	GGA
a (Å)	5.46	5.53	5.69
α (°)	60.2	59.7	59.1
E_g^{KS} (eV)	0.4	2.0	0.9
M_{Fe} (μ_B)	3.4	4.0	3.7

10^{-4} Ha/bohr (∼0.02 eV/Å) on the maximal forces. Also, a $3 \times 3 \times 3$ supercell (270 atoms) was used in selected cases, within LDA+U, to ensure that the 80-atom supercell used is large enough and does not induce spurious finite-size effects that would alter the physics. These additional calculations were performed using a plane-wave cutoff of 20 Ha and the Γ point only to sample the corresponding Brillouin zone, they are presented in Appendix A. The defects recomputed in this 270-atom supercell are the three monovacancies (Bi, Fe, O) and one Bi-O vacancy pair ($[\mathrm{Bi}-\mathrm{O}]_1$), in their possible charge states. Except when explicitly mentionned, the results presented in the main text refer to the 80-atom supercell.

Perfect BFO in its ground-state structure (rhombohedral $R3c$ space group, G-type AFM) has been first optimized in its ten-atom primitive cell for LDA, LDA + U, and GGA-PBE. The structure of BFO results from a set of distortions of the parent cubic perovskite structure, corresponding to oxygen octahedra rotating in antiphase about each axis (by the same angle, in Glazer notation $a^-a^-a^-$), superimposed to large FE displacements. The lattice constants, KS band gap E_g^{KS}, and spin magnetic moments on iron atoms obtained after relaxation are summarized in Table I, and show good agreement with earlier works, both for LDA and LDA+U [41], as well as for GGA [44–47]. In LDA+U, we find the following optimized atomic positions: Bi(2a)(x,x,x) with x = 0; Fe(2a)(x,x,x) with x = 0.225; O(6b)(x,y,z) with x = 0.540, y = 0.939, z = 0.394.

Most results presented in this work have been obtained in LDA+U (this denotation will refer here to U being applied on Fe d orbitals). However, if such scheme describes rather well the correlation effects associated with 3d electrons of Fe, it is not able to correct the self-interaction error that may affect the 2p electrons of oxygen and that is known to hinder the simulation of oxygen-type self-trapped hole polarons within LDA. A practical way to achieve such correction is to add an extra U on the p orbitals of oxygen. We will use such simulation scheme in Sec. VI B and will denote it as LDA+U + U_p.

C. Formation energies of the defects

In this work, we have simulated single vacancies and Bi-O/Fe-O divacancies in the 80-atom supercell with different charge states q. The numerical values given hereafter correspond, except when explicitly mentioned, to LDA+U calculations. The formation energy of a M vacancy (M = Bi, Fe, O) in a supercell with charge state q is computed, according to the standard scheme, as

$$\Delta E_f(\mathrm{V}_M, q) = E_{\mathrm{tot}}(\mathrm{BFO} + \mathrm{V}_M, q) - E_{\mathrm{tot}}(\mathrm{BFO}) + \mu_M + q\mu_e, \quad (1)$$

in which $E_{\mathrm{tot}}(\mathrm{BFO} + \mathrm{V}_M, q)$, $E_{\mathrm{tot}}(\mathrm{BFO})$, μ_M, and μ_e are, respectively, the total energy of the BFO supercell containing the M vacancy with charge state q, the total energy of a perfect undefective BFO supercell, the chemical potential of chemical species M, and the chemical potential of the electrons (Fermi level).

The chemical potential of species M is referred to the standard state (solids Bi and Fe, molecular O_2), according to $\mu_M = E_{\mathrm{tot}}(M, \mathrm{std}) + \Delta\mu_M$ [$E_{\mathrm{tot}}(M, \mathrm{std})$ is the total energy of chemical species M in its standard state], while that of the electrons is referred to the valence band maximum E_{VBM}: $\mu_e = E_{\mathrm{VBM}} + \epsilon_F$, ϵ_F varying between 0 and the band gap E_g. The chemical potentials of Bi, Fe, and O are subject to constraints driven by the existence of $BiFeO_3$, the nonformation of the pure solids Bi and Fe, and the nonformation of the binary sesquioxides Bi_2O_3 and Fe_2O_3:

$\Delta\mu_{Bi} \leqslant 0$; $\Delta\mu_{\mathrm{Fe}} \leqslant 0$;

$2\Delta\mu_{Bi} + 3\Delta\mu_O \leqslant E_f(Bi_2O_3)$ (formation energy of Bi_2O_3);

$2\Delta\mu_{\mathrm{Fe}} + 3\Delta\mu_O \leqslant E_f(Fe_2O_3)$ (formation energy of Fe_2O_3);

$\Delta\mu_{Bi} + \Delta\mu_{\mathrm{Fe}} + 3\Delta\mu_O = E_f(BFO)$ (formation energy of BFO).

These inequalities express respectively the nonformation of solids Bi and Fe, the nonformation of the binary oxides Bi_2O_3 and Fe_2O_3, while the last equality expresses the stability of bismuth ferrite. Following Ref. [18], we consider $\Delta\mu_{Bi}$ and $\Delta\mu_{\mathrm{Fe}}$ as the independent variables that control the chemical state of the system, the oxygen chemical potential $\Delta\mu_O$ being related to them by the last equality.

The energy of the valence band maximum (VBM) E_{VBM} is determined directly from the electronic density of states (e-DOS) of perfect BFO, and also by comparing the total energy of the perfect supercell with and without a (band) hole. Both values are found to agree within 1 mHa. The energy of the conduction band minimum (CBM), E_{CBM}, may be determined in the same manner, by comparing the total energy of the perfect supercell with and without a (band) electron. This provides a fundamental band gap of 2.05 eV, close to the KS band gap observed in the e-DOS.

The defects simulated in a globally neutral supercell (q = 0) will be denoted in this work as *charge-neutral* defects [18,40], while those simulated in a supercell with $q \neq 0$ will be denoted as *ionized* (when they reach their maximal possible charge state), or *partially ionized* otherwise. Here, the vacancies simulated in a neutral supercell are associated with the release of electronic charges (electrons or holes) that are found to be localized around the defect or in its vicinity.

The transition energy level between a defect (here a M vacancy) in charge state q and the same defect in charge state q' is defined by

$$\epsilon_{\mathrm{V}_M}(q/q') = \frac{\Delta E_f(\mathrm{V}_M, q; \epsilon_F{=}0) - \Delta E_f(\mathrm{V}_M, q'; \epsilon_F{=}0)}{q' - q}, \quad (2)$$

where $\Delta E_f(\mathrm{V}_M, q; \epsilon_F = 0)$ is the formation energy of vacancy $\mathrm{V_M}$ in charge state q, calculated for the Fermi level at the VBM [58]. $\epsilon_{\mathrm{V}_M}(q/q')$ corresponds to the Fermi level at which the formation energies of the defect in charged states q and q' cross.

Charged supercells are simulated by adding/removing electrons and compensating their charge with a uniform background (jellium), according to the usual scheme. In the calculation of defect formation energies, the total energies for the charged supercells are corrected using the monopole part of the Makov-Payne correction [59] (with $\epsilon_S = 22$ as static dielectric constant [53], a value close to that obtained from molecular dynamics simulations in Ref. [60]– ∼30 —and from experiments [61]) and by a band alignment onto the density of states of the perfect stoichiometric system, in order to compensate for the loss of reference of the average potential when using the jellium. This alignment is performed using localized semicore levels (Fe 3*s*), as in Ref. [62].

D. Defect model

We set up a simple model in order to estimate the concentration in the different defects and free charges, and equilibrium Fermi level [63]. The concentration of free electrons (respectively, holes) is assumed to be $n = N_c(T)e^{-\frac{E_g-\epsilon_F}{k_BT}}$ [respectively, $p = N_v(T)e^{-\frac{\epsilon_F}{k_BT}}$, we recall that ϵ_F is referenced to the VBM], with $N_c(T) = 2(\frac{2\pi m_e^* k_B T}{h^2})^{3/2}$ and $N_v(T) = 2(\frac{2\pi m_h^* k_B T}{h^2})^{3/2}$. For simplicity, we take the effective masses m_e^* and m_h^* equal to the electron mass (the results are not deeply modified when these parameters are changed by a factor 10 or 1/10). We take $E_g = 2.7$ eV for the band gap.

The Fermi level at equilibrium, $\epsilon_F^{\rm eq}$, may be obtained by solving the electroneutrality equation, assuming that (i) the vacancies here considered (Bi, Fe, O) are the main defects in the system (with possible charge states for cation vacancies 3−, 2−, 1−, 0, and for O vacancies 2+, 1+, 0) and (ii) free holes and free electrons, once escaped from the defects (i.e., once the defects are ionized), are itinerant (occupying band states, i.e., self-trapped polarons are not considered, at least in a first time):

$$n + 3\left[\mathrm{V}_{\mathrm{Bi}}^{3-}\right] + 2\left[\mathrm{V}_{\mathrm{Bi}}^{2-}\right] + \left[\mathrm{V}_{\mathrm{Bi}}^{1-}\right] + 3\left[\mathrm{V}_{\mathrm{Fe}}^{3-}\right] + 2\left[\mathrm{V}_{\mathrm{Fe}}^{2-}\right] + \left[\mathrm{V}_{\mathrm{Fe}}^{1-}\right] = p + 2\left[\mathrm{V}_{\mathrm{O}}^{2+}\right] + \left[\mathrm{V}_{\mathrm{O}}^{1+}\right]. \quad (3)$$

The concentration of M vacancies in charge state q is $[\mathrm{V}_M^q] = [M]e^{-\frac{\Delta E_f(V_M,q)}{k_BT}}$. Numerical applications are done hereafter for $T = 300$ K.

III. ENERGETICS OF THE DEFECTS

The formation energies of defects are calculated in two different external conditions, namely the same as those chosen by Paudel *et al.* [18], which correspond to strong oxidative or reducing conditions: (i) oxidative conditions: $\Delta\mu_O = -0.5$ eV ($\Delta\mu_{Bi} = -3.19$ eV; $\Delta\mu_{\mathrm{Fe}} = -4.29$ eV) and (ii) reducing conditions: $\Delta\mu_O = -2.0$ eV ($\Delta\mu_{Bi} = -0.94$ eV; $\Delta\mu_{\mathrm{Fe}} = -2.04$ eV). In each case, $\Delta\mu_{Bi}$ and $\Delta\mu_{\mathrm{Fe}}$ are chosen exactly at the middle of the interval allowed by the nonformation of elemental solids and binary oxides.

A. Isolated vacancies

Figure 2 displays the formation energies of the isolated vacancies, as a function of the Fermi level, for the two regimes described above. They are in rather good qualitative agreement with the results of Paudel *et al.* [18] and Shimada *et al.* [40]. The formation energy of the electron polaron is also superimposed to the oxygen vacancy case. Cationic vacancies are acceptor defects, associated with holes. Either the holes are released in the lattice (as delocalized in a band state or as a self-trapped polaron, or are trapped by another (donor) defect), or they remain trapped close to the vacancy. The hallmark of such a release is the existence of the vacancy in a partially ionized or fully ionized state: in the charge-neutral state, the holes are usually localized and trapped close to the defect (see Sec. IV).

In oxygen-rich conditions, we expect the equilibrium Fermi level $\epsilon_F^{\rm eq}$ to be rather close to the VBM, so that charge-neutral or partially ionized cation vacancies may coexist with ionized oxygen vacancies ($\mathrm{V}_{\mathrm{O}}^{2+}$). This would probably be the case in extremely oxidizing conditions such as $\Delta\mu_O = 0$. However, in the oxidative conditions here chosen, our simple defect model provides $\epsilon_F^{\rm eq} = 0.74$ eV. Free holes largely dominate over free electrons ($p \gg n$), with charge compensation being ensured by Bi and Fe vacancies (mostly ionized and partially ionized Bi vacancies). The most stable state for V_{Bi} for such Fermi level is the fully ionized one, $\mathrm{V}_{\mathrm{Bi}}^{3-}$, indicating that the Bi vacancies have been ionized and have released their holes, which may thus contribute to *p*-type conduction. Thus, hole-type conductivity may be expected in these oxidative conditions (provided the effective masses of electrons and holes do not differ by orders of magnitude).

In oxygen-poor conditions ($\Delta\mu_O = -2.0$ eV), in contrast, the equilibrium Fermi level lies much higher in the band gap: the defect model provides $\epsilon_F^{\rm eq} = 1.30$ eV, showing that oxygen vacancies are mostly either fully ionized ($\mathrm{V}_{\mathrm{O}}^{2+}$) or partially ionized ($\mathrm{V}_{\mathrm{O}}^{1+}$), but not neutral. More precisely, the number of neutral O vacancies is found smaller than that of ionized/partially ionized ones by 5 orders of magnitude. The system remains, however, rather *p*-type, with a concentration of free holes larger than that of free electrons by a factor ∼60. Most of these holes are compensated (and thus have been released) by ionized Bi vacancies, which have approximately the same concentration as that of free holes: $3[\mathrm{V}_{\mathrm{Bi}}^{3-}] \approx \mathrm{p} \gg [\mathrm{V}_{\mathrm{O}}^{1+}] \approx [\mathrm{V}_{\mathrm{O}}^{2+}] \gg [\mathrm{V}_{\mathrm{O}}^{0}]$. The most favorable state for the Fe vacancy in such conditions is the ionized one: ionized Fe vacancies are in concentration close to that of $\mathrm{V}_{\mathrm{O}}^{2+}$ and $\mathrm{V}_{\mathrm{O}}^{1+}$. The concentration of free electronic carriers (mostly holes) is here smaller than in oxygen-rich conditions by about ten orders of magnitude.

Table II displays the transition energy levels between stable charge states for the three vacancies. The transition levels for the O vacancy [+2/+1: 1.31 eV, +1/0: 1.56 eV] (+2/+1: 1.41 and +1/0: 1.65 eV using the $3 \times 3 \times 3$ supercell) are in good agreement with the LDA+U calculation of Paudel *et al.* [18], and comparable to the ones obtained by Clark and Robertson by screened-exchanged calculations [39], although our value is somewhat lower, and also lower than the one

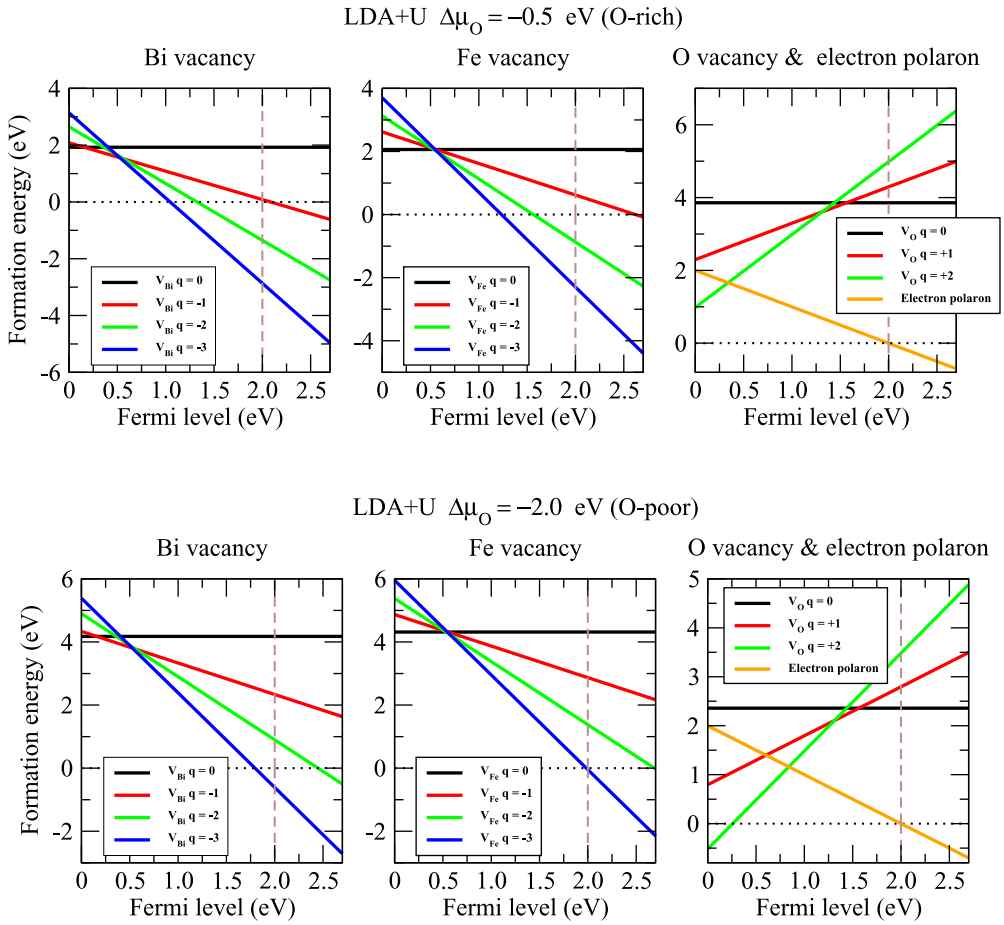

FIG. 2. Formation energies of the isolated vacancies calculated with LDA+U, in oxygen-rich conditions (upper panels, $\Delta\mu_O = -0.5$ eV) and oxygen-poor conditions (lower panels, $\Delta\mu_O = -2.0$ eV). Dashed brown vertical line: LDA+U band gap.

obtained by Shimada *et al.* using HSE06 hybrid functional (2.18 and 2.38 eV) [40]. Note that this latter discrepancy may be an effect of the inaccurate band gap description in the present LDA+U scheme (it is underestimated by ∼0.7 eV). If we assume the VBM as relatively well described and this error coming mostly from the position of the CBM, we may adjust the CB by a rigid shift, by 0.7 eV to recover the experimental gap. Then the transition energies would be shifted by ∼0.7 eV, to ∼2.01 and 2.26 eV (2.11 and 2.35 eV using the $3 \times 3 \times 3$ supercell), in much better agreement with Shimada's values [40].

Our values lead to the conclusion that V_O is a moderately deep double donor. The transition levels for the Bi (respectively, Fe) vacancy are rather small, they range from 0.16 to 0.53 eV (respectively, 0.53 to 0.58 eV), in rather good agreement with the LDA+U calculations of Paudel *et al.*, [18] who concluded that such levels are easy to ionize, thus releasing holes and contributing to p-type conductivity. The present results for V_{Bi} are also similar to the GGA calculation of Xu *et al.* [19]. The HSE06 calculations of Shimada *et al.* [40] lead to a smaller (respectively, higher) transition level 0.08 eV (respectively, 0.83 eV) above the VBM for the Bi (respectively, Fe) vacancy, providing for V_{Bi} (respectively, V_{Fe}) the picture of a triple shallow (respectively, triple deep) acceptor. Owing to the broad range of oxygen chemical potentials investigated here, BFO is thus expected to be mostly a p-type oxide in oxygen-rich conditions and exhibit only a small concentration of free charge carriers in oxygen-poor conditions.

TABLE II. Transition energy levels (in eV) between stable charge states for the three vacancies and the divacancies.

V_O	V_{Bi}	V_{Fe}	$V_{[Bi\text{-}O]_1}$	$V_{[Fe-O]_2}$
$\epsilon_{V_O}(+2/+1) = 1.31$	$\epsilon_{V_{Bi}}(0/-1) = 0.16$	$\epsilon_{V_{Fe}}(0/-2) = 0.53$	$\epsilon_{V_{[Bi\text{-}O]_1}}(+2/+1) = 0.05$	$\epsilon_{V_{[Fe-O]_2}}(+2/+1) = 0.13$
$\epsilon_{V_O}(+1/0) = 1.56$	$\epsilon_{V_{Bi}}(-1/-3) = 0.53$	$\epsilon_{V_{Fe}}(-2/-3) = 0.58$	$\epsilon_{V_{[Bi\text{-}O]_1}}(+1/0) = 0.24$	$\epsilon_{V_{[Fe-O]_2}}(+1/0) = 0.29$
			$\epsilon_{V_{[Bi\text{-}O]_1}}(0/-1) = 0.39$	$\epsilon_{V_{[Fe-O]_2}}(0/-1) = 0.44$
			$\epsilon_{V_{[Bi\text{-}O]_1}}(-1/-2) = 1.76$	$\epsilon_{V_{[Fe-O]_2}}(-1/-2) = 1.98$
			$\epsilon_{V_{[Bi\text{-}O]_1}}(-2/-3) = 2.15$	$\epsilon_{V_{[Fe-O]_2}}(-2/-3) = 2.28$

TABLE III. Cation-oxygen distances (in Å) in the perfect BFO crystal, in the different configurations of the divacancy, and angle between the [111] direction (direction of the polarization) and the divacancy dipole.

Vacancy pair	Bi-O (Å) GGA	[111]-Bi-O (°) GGA	Bi-O (Å) LDA+U	[111]-Bi-O (°) LDA+U
$[Bi\text{-}O]_1$	2.37	42.7	2.29	42.7
$[Bi\text{-}O]_2$	2.48	103.8	2.42	103.8
$[Bi\text{-}O]_3$	3.31	100.3	3.21	100.4
$[Bi\text{-}O]_4$	3.42	148.8	3.33	148.7
Vacancy pair	Fe-O (Å) GGA	[111]-Fe-O (°) GGA	Fe-O (Å) LDA+U	[111]-Fe-O (°) LDA+U
$[Fe\text{-}O]_1$	2.15	131.6	2.07	131.4
$[Fe\text{-}O]_2$	1.99	62.9	1.94	62.6

B. Divacancies

We now remove two atoms (M and O, M = Bi or Fe) from the supercell to simulate a cation/anion divacancy, in different charge states. The formation energy of the M-O divacancy in charge state q is still defined according to

$$\Delta E_f(\mathrm{V}_{[\mathrm{M-O}]}, q) = E_{\mathrm{tot}}(\mathrm{BFO} + \mathrm{V_M} + \mathrm{V_O}, q) - E_{\mathrm{tot}}(\mathrm{BFO}) + \mu_M + \mu_O + q\mu_e. \quad (4)$$

Then we define the association energy of the two defects by

$$E_{\mathrm{int}}(\mathrm{V_M} - \mathrm{V_O}, q_1 + q_2) = \Delta E_f(\mathrm{V}_{[\mathrm{M-O}]}, q_1 + q_2) - \Delta E_f(\mathrm{V_M}, q_1) - \Delta E_f(\mathrm{V_O}, q_2). \quad (5)$$

$E_{\mathrm{int}} < 0$ means that the two defects have the tendency to attract and form clusters. We restrict ourselves to the removal of an oxygen located in the first coordination shell of the cation, and to an oxygen removed farther away in the supercell (configurations hereafter called $[Bi\text{-}O]_{\mathrm{far}}$ and $[Fe\text{-}O]_{\mathrm{far}}$). However, due to the symmetry restrictions of the host BFO compound, this leads to five cases in the case of Bi/O (four possibilities in the first coordination shell + the oxygen further removed) and three cases in the case of Fe/O (two possibilities in the first coordination shell + the oxygen further removed), which are described hereafter. The charge states of the divacancy are studied from $q = +2$ to $q = -3$.

1. Bi-O divacancy

In the centrosymmetric $Pm\bar{3}m$ perovskite structure ABO_3, the A ion is surrounded by 12 oxygen atoms. When the structure is distorted, these 12 atoms may become nonequivalent *with respect to the A site*, and located at different distances from A. In the rhombohedral phase of BFO, they are split into four subgroups of three atoms (equivalent with respect to a given Bi), placed at 2.29, 2.42, 3.21, and 3.33 Å from this Bi atom. We denote the corresponding pairs as $[Bi\text{-}O]_1$, $[Bi\text{-}O]_2$, $[Bi\text{-}O]_3$, and $[Bi\text{-}O]_4$ (see Table III). Thus, even by restricting to this first coordination shell, there are four possible states of the Bi-O divacancy defect, which differ (i) by the Bi-O distance between the removed atoms, and thus the electric dipole of the divacancy, and (ii) the angle between this dipole and the bulk polarization. Another position was computed, corresponding to vacancies farther away from each other in the supercell (Fig. 3). Note that in any case, the defect dipole always lies from the missing cation (negatively charged defect) to the missing oxygen (positively charged defect).

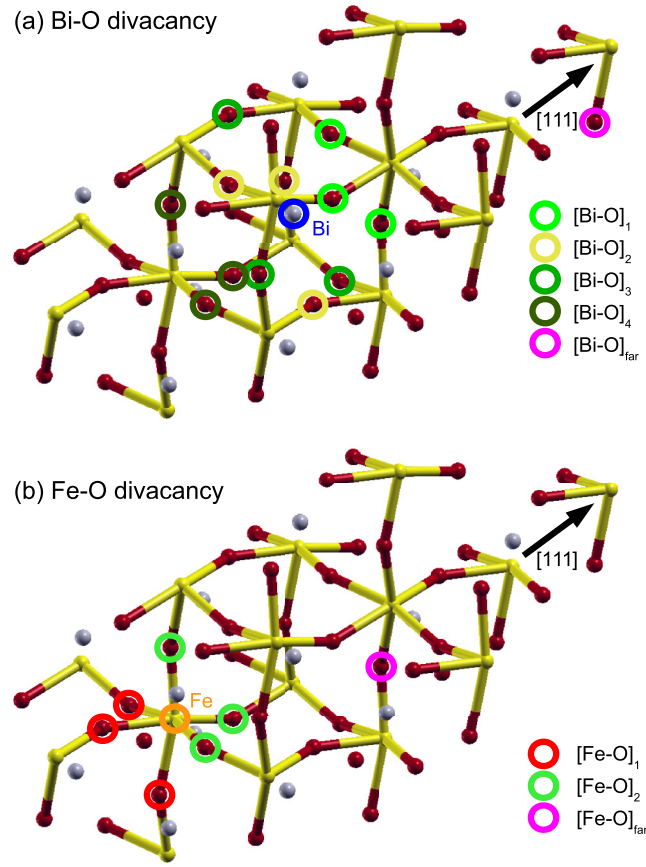

FIG. 3. (a) The four subsets of oxygen atoms around the Bi atom in $R3c$ BFO. The Bi-O divacancy is simulated in four configurations, each one corresponding to the removal of one oxygen in a given subset. (b) The two subsets of oxygen atoms around the Fe atom in $R3c$ BFO. The Fe-O divacancy is simulated in two configurations, each one corresponding to the removal of one oxygen in a given subset. Bi, Fe, and O atoms are respectively in grey, yellow, and red.

Among the six possible charge states of this bidefect, three appear as stable over an appreciable range of Fermi levels: $q = 2$, -1, and -3 (see Fig. 4). $q = 2$ can be seen as the association of $\mathrm{V_{Bi}^0}$ and $\mathrm{V_O^{2+}}$ (ϵ_F close to VBM), while $q = -3$ can be seen as the association of $\mathrm{V_{Bi}^{3-}}$ and $\mathrm{V_O^0}$ (ϵ_F close to CBM). $q = -1$ corresponds to the association of the fully ionized vacancies, $\mathrm{V_{Bi}^{3-}}$ and $\mathrm{V_O^{2+}}$ (ϵ_F within the band gap).

The two most stable divacancies are $\mathrm{V}_{[\mathrm{Bi\text{-}O}]_1}$ and $\mathrm{V}_{[\mathrm{Bi\text{-}O}]_2}$. They correspond to the shortest oxygen/Bi distance (2.29 and 2.42 Å). The two other possible configurations, $\mathrm{V}_{[\mathrm{Bi\text{-}O}]_3}$ and $\mathrm{V}_{[\mathrm{Bi\text{-}O}]_4}$, correspond indeed to much larger oxygen/Bi distances (3.21 and 3.33 Å), i.e., ∼1 Å larger. This suggests that the two vacancies attract each other. In the most stable $\mathrm{V}_{[\mathrm{Bi\text{-}O}]_1}$ and $\mathrm{V}_{[\mathrm{Bi\text{-}O}]_2}$ configurations, the dipole associated with the bidefect makes an angle of 42.7 and 103.8°, respectively, with the direction of the polarization, whereas this angle is 100.3 and 148.8° in the case of $\mathrm{V}_{[\mathrm{Bi\text{-}O}]_3}$ and $\mathrm{V}_{[\mathrm{Bi\text{-}O}]_4}$, respectively.

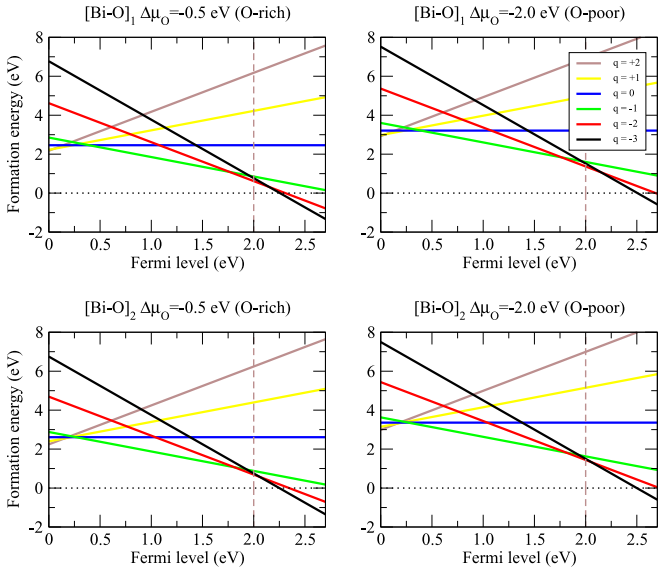

FIG. 4. Formation energies of the $[\text{Bi-O}]_1$ and $[\text{Bi-O}]_2$ divacancies, in oxygen-rich (left) and oxygen-poor (right) conditions, for charge states from $q = -3$ to $+2$. Dashed brown vertical line: LDA+U band gap.

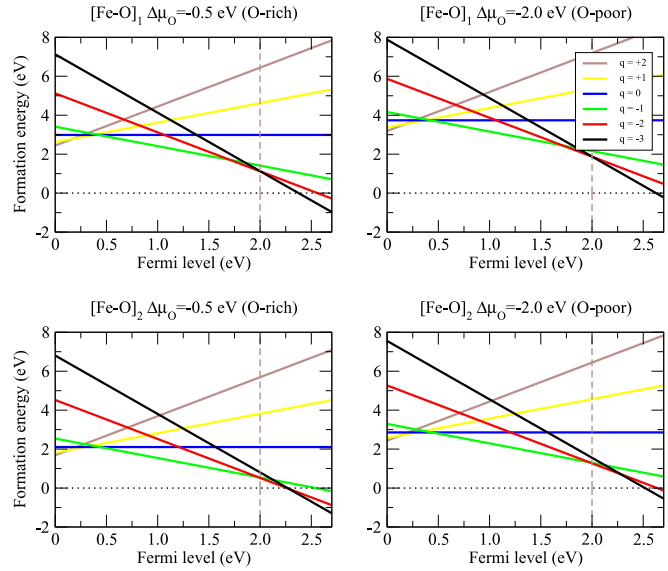

FIG. 5. Formation energies of the $[\text{Fe-O}]_1$ and $[\text{Fe-O}]_2$ divacancies, in oxygen-rich (left) and oxygen-poor (right) conditions, for charge states from $q = -3$ to $+2$. Dashed brown vertical line: LDA+U band gap.

The plot of the formation energies in Fig. 4 as a function of Fermi level (in oxidative and reducing conditions), reveals the transition energy levels for this bidefect in configurations $V_{[\text{Bi-O}]_1}$ and $V_{[\text{Bi-O}]_2}$; they are summarized in Table II for $V_{[\text{Bi-O}]_1}$. We observe transition levels closer to the VBM, and also closer to the CBM, than in the case of isolated vacancies, indicating that the divacancy may behave as a rather shallow acceptor, or as a donor according to the Fermi level. Moreover, the charge state $q = -1$, which corresponds to the association of both fully ionized defects (V_{Bi}^{3-} and V_O^{2+}), possesses a stability domain, from 0.39 to 1.76 eV (0.44 to 1.84 eV using the $3 \times 3 \times 3$ supercell), much larger than that of the same charge states for the corresponding isolated vacancies. For example, at $\epsilon_F = 1.70$ (respectively, 0.45) eV, the Bi (respectively, oxygen) vacancy is in charge state V_{Bi}^{1-} (respectively, V_O^0), whereas in the bidefect, the two vacancies are fully ionized. This may be easily understood since the two defects at short distance undergo more easily a charge transfer than far from each other, just like two atoms in an ionic molecule. As a result, the acceptor transition levels are globally shifted towards the VBM, while the donor transition levels are shifted towards the CBM. Moreover, if we refer to the LDA+U band gap (∼2 eV), we would conclude that the latter levels are shallow.

2. Fe-O divacancy

The case of the Fe/O divacancy is more simple, since in the $R3c$ structure of BFO the six oxygen atoms surrounding a given Fe are split into two subgroups of three atoms equivalent with respect to this Fe atom, located at 2.07 ($[\text{Fe-O}]_1$) and 1.94 Å($[\text{Fe-O}]_2$) from Fe. The $V_{[\text{Fe-O}]_2}$ configuration is found to be much more stable than $V_{[\text{Fe-O}]_1}$. It corresponds to the shortest Fe-O distance, and to an angle of 62.6° between the electric dipole formed by the Fe-O pair and the direction of the polarization (versus 131.4° for $[\text{Fe-O}]_1$). Here again, another position was computed, corresponding to vacancies far away from each other in the supercell (Fig. 3), and found to be less stable than $V_{[\text{Fe-O}]_1}$ and $V_{[\text{Fe-O}]_2}$, irrespective of the charge state.

The formation energies of $V_{[\text{Fe-O}]_1}$ and $V_{[\text{Fe-O}]_2}$ are plotted in Fig. 5 as a function of Fermi level, in oxidative and reducing conditions. Exactly the same trend as for the Bi-O divacancy is observed, the Fe-O bidefect being either a rather shallow acceptor or a donor according to the value of ϵ_F. Here again, the stability domain of the charge state $q = -1$ (from 0.44 to 1.98 eV), which corresponds to the association of the fully ionized defects V_{Fe}^{3-} and V_O^{2+}, is enlarged compared to that of the same charge states for the isolated vacancies (Table II).

3. Association energies

Using the stability domains of the monovacancies in terms of Fermi level, as well as the spin of the system, it is possible to identify the charge states q_1 and q_2 of the two vacancies involved in the pair with charge $q = q_1 + q_2$ (Table IV). Figure 6 displays the association energies of the Bi-O and Fe-O divacancies as a function of the total charge state of the bidefect q, and for each configuration studied.

Firstly, these energies are almost always negative, indicating that the two vacancies attract each other in most configurations and charge states. They are, moreover, globally more negative in the first-neighbor shell than far from each other (except for $[\text{Bi-O}]_3$).

Secondly, they are all maximum (in absolute value), i.e., the attraction is the strongest, for the charge state $q = -1$, which corresponds to the association of two fully ionized vacancies, $V_{Bi/Fe}^{3-}$ and V_O^{2+}. The strongest interaction being associated with vacancies of maximal charge state, this attraction is suggested to be mainly electrostatic in nature. The strong, stabilizing, interaction for $q = -1$ explains, moreover, why the stability domain of this charge state is enlarged as

TABLE IV. Charge states q_1 and q_2 of the two monovacancies (respectively, cation and oxygen) involved in the divacancy of total charge $q = q_1 + q_2$. Between [...]: spin magnetic moment (μ_B) of the defective supercell with monovacancy (second column: with cation monovacancy; third column: with oxygen monovacancy). Last column: spin magnetic moment (μ_B) of the defective supercell with the divacancy ($V_{[Bi-O]}/V_{[Fe-O]}$).

q	$q_1(V_{Bi/Fe})$	$q_2(V_O)$	Configuration	Spin
2	0 [1.15/2]	2 [0]	$V^{0}_{Bi/Fe}$-V^{2+}_{O}	1/2
1	−1 [2/3]	2 [0]	$V^{1-}_{Bi/Fe}$-V^{2+}_{O}	0/3
0	−2 [1/4]	2 [0]	$V^{2-}_{Bi/Fe}$-V^{2+}_{O}	1/4
−1	−3 [0/5]	2 [0]	$V^{3-}_{Bi/Fe}$-V^{2+}_{O}	0/5
−2	−3 [0/5]	1 [1]	$V^{3-}_{Bi/Fe}$-V^{1+}_{O}	1/4
−3	−3 [0/5]	0 [0]	$V^{3-}_{Bi/Fe}$-V^{0}_{O}	0/5

compared to that of the corresponding fully ionized isolated vacancies.

Third, the association energies are rather strong. For the association of the two fully ionized vacancies ($q = -1$), they reach $\sim$−1.2/−1.3 eV for $V_{[Bi-O]_1}$ and $V_{[Bi-O]_2}$, and $\sim$−2.1 eV for $V_{[Fe-O]_2}$. This is not surprising since this corresponds to the interaction between a defect of charge +2 and another one of charge −3. For low Fermi levels, the most stable charge state of the divacancy is $q = 2$, it corresponds to the association of a charge-neutral Bi/Fe vacancy, $V^{0}_{Bi/Fe}$, and an ionized oxygen vacancy, V^{2+}_{O}. The association energy is here $\sim$−0.7 eV for $[Bi - O]_1$ and $[Bi - O]_2$, and −1.4 eV for $[Fe - O]_2$. Note that charge compensation between the bidefect and the isolated ones makes the association energies independent from the external (oxygen chemical potential) and internal (Fermi level) conditions.

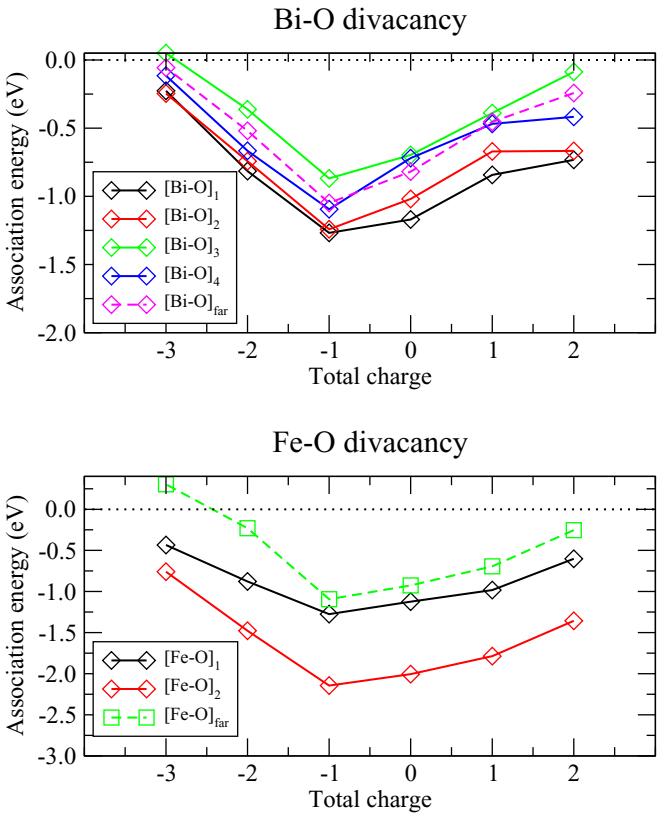

FIG. 6. Association energies of the Bi-O vacancy pair (top) and Fe-O vacancy pair (bottom), as a function of the total charge of the bidefect, and for the different configurations studied.

IV. ELECTRONIC STATES ASSOCIATED TO THE DEFECT

The point defects studied here are associated with defect states lying within the band gap. We now scrutinize the e-DOS of defective BFO, and the KS quantum states associated to the defects. These defect states, which typically lie in the band gap and are usually spatially localized, are denoted herafter as *up1*, *dn1*, etc., whether they are obtained in our calculation with spin up or down, and ordered by increasing energy (following the notations of Ref. [40]). These KS states in the band gap must not be confused with the transition energy levels previously described. The KS states are not able to provide information about the stable charge state of the defect for a given Fermi level (in contrast to the transition energy levels), but they contain information about the spatial localization and orbital character of the extra charges associated to the defect. For each defect, we describe how the defect states evolve with charge state, and then characterize the associated electronic or hole polarons. For each monovacancy, we display the GGA-PBE and LDA+U e-DOS, with the zero of energies placed approximately at mid-distance between the highest occupied and the lowest unoccupied KS states (note that the 0-K Fermi energy, which corresponds to the energy of the highest occupied KS state in the electronic ground state, and makes sense only for the defect configuration considered, must not be confused with the Fermi level previously used). In selected cases, an isosurface of the density of probability of the defect state is plotted, for a value equal to 1/5 of the maximum value.

A. Oxygen vacancy

The oxygen vacancy in BFO is associated with two defect states within the band gap (Fig. 7). LDA+U and GGA qualitatively drive the same description of these states.

1. Defect states

The charge-neutral oxygen vacancy V^{0}_{O} is a double donor defect, which is corroborated by the presence of two occupied states, with opposite spin, approximately located in the middle of the KS band gap (denoted as *up1* and *dn1* on Fig. 7). The density of probability of these states is shown in Fig. 8: each one is mostly localized on one of the two Fe atoms surrounding the vacancy, and has thus a marked Fe 3d character. Each one is, however, strongly polarized towards the vacancy, as a consequence of the Madelung potential (note that in purely ionic crystals, oxygen vacancies are commonly "color centers," the released electrons being localized *in* the vacancy). Here the Madelung potential is not sufficient to maintain the two electrons inside the vacancy, but is enough to strongly polarize the two states. The two electrons released are thus localized on the two Fe surrounding the vacancy, under the form of two trapped small polarons. Each state is spin-polarized, but the charge-neutral vacancy is not, since both states with opposite spin are occupied. This description agrees well with previous *ab initio* works [39,40].

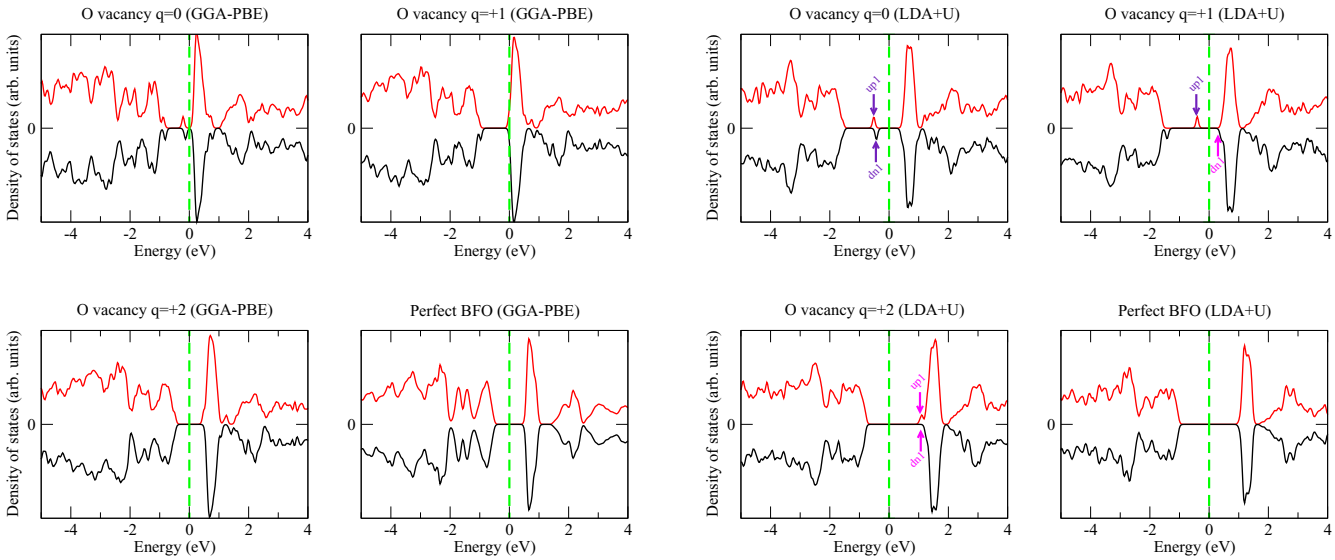

FIG. 7. e-DOS for the three charge states of the O vacancy, as obtained from GGA and LDA+U. The zero of energy is placed approximately at mid-distance between the highest occupied and the lowest unoccupied state (dashed green vertical line). The arrows indicate where the defect states lie. The neutral O vacancy (double donor) generates two occupied states with opposite spin lying approximately in the middle of the band gap. Upon charging positively the vacancy, these states become unoccupied and their energy raises up to the bottom of the conduction band. Positive/red curves: spin ↑, negative/black curves: spin ↓. Small violet (respectively, magenta) arrows: occupied (respectively, unoccupied) KS defect states.

Formally, the localization of the two electrons on the neighboring Fe atoms corresponds to a reduction of these two Fe^{3+} ions into Fe^{2+}. Since the Fe^{3+} in BFO are in the high-spin state, the supplementary electron has necessarily a spin opposed to that of the Fe^{3+} ion: for instance, a Fe^{3+} in state $(3d^5_\uparrow, 3d^0_\downarrow)$ becomes, upon reduction, Fe^{2+}, in state $(3d^5_\uparrow, 3d^1_\downarrow)$. Consequently, the spin magnetic moment of each reduced Fe is decreased: 3.7 μ_B (versus 4.0 μ_B in perfect BFO in LDA+U). The two defect states associated with the O vacancy therefore have opposite spins, and the two Fe^{2+} that surround the vacancy remain antiferromagnetically coupled.

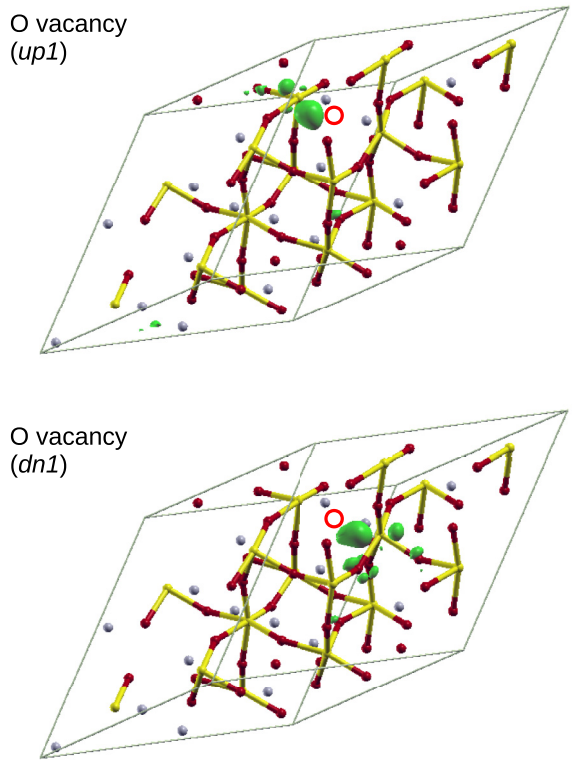

FIG. 8. Isosurfaces of the density of probability of the two defect states associated to the charge-neutral oxygen vacancy (LDA+U). The position of the O vacancy is shown with a red circle. The two states are occupied. The straight grey lines are the edges of the 80-atom supercell.

Finally, we note that the two reduced Fe ions are not equivalent with respect to the missing O atom, because the two Fe-O distances are not equal owing to the FE distortion. This explains why the two defect states have not exactly the same energy (Fig. 7).

In the 1+ charge state, one of the two defect states (here *dn1*) becomes empty. Its energy increases and comes just at the edge of the CBM. This empty state keeps a strong density of probability on the Fe close to the vacancy (the one on which it is when occupied), but also hybridizes to empty 3*d* orbitals of other Fe atoms, coming from the conduction band. In the 2+ charge state, the second defect state (*up1*) is also emptied and joins the CBM as well, a behavior common to various oxides, such as ZnO [64]. *up1* remains, however, rather well localized on the Fe (close to the vacancy) on which it is when occupied. Calculations using a $3 \times 3 \times 3$ supercell confirm this evolution of the defect states upon charging the defect (see Appendix A).

2. *Isolated electron polaron*

The question remains whether the electronic carriers released by the oxygen vacancies after ionization, in the hypothesis that they are not captured by other point defects, localize in the form of small polarons far from the defect, or whether

they are delocalized in Bloch-like states. In order to address that question, we simulated an isolated self-trapped electron polaron, using the methodology described in Ref. [69] (details are given in Appendix B); essentially, this is achieved by adding an extra electron into the undefective supercell, forcing its localization on one Fe atom, and structurally optimizing the system. At the end, the electron is "self-trapped" on this Fe, i.e., it is localized on it, with a "self-trapping" distortion all around; indeed, we observe that the electron polaron distorts the crystal in its neighborhood, with the two Fe-O distances being enhanced to 2.00 and 2.13 Å (versus 1.94 and 2.07 Å in the perfect crystal), in agreement with the charge on the Fe ion decreasing formally from +3 to +2. This Fe atom is thus formally in oxidation state +2 (its spin magnetic moment falls to $\sim 3.5\,\mu_B$), and the extra electron occupies a $3d$ orbital of the minority spin channel, owing to the high-spin state of Fe^{3+} (see Sec. VI A).

The corresponding occupied minority spin state is found to lie within the band gap, at only ∼0.3 eV below the CBM. However, the self-trapped polaronic state has an energy larger than that of the free electron state (in which the electron occupies a band state in the perfect, undistorted crystal) by 0.15 eV, indicating that, in the present numerical scheme, free electrons are more stable in delocalized band states rather than as small polarons. This fact is consistent with the formation energy of the electron polaron crossing zero at $\epsilon_F \sim 2.0$ eV (Fig. 2), which roughly corresponds to the KS band gap of BFO in the present LDA+U calculations.

The charge-neutral (respectively, singly ionized) O vacancy may also be seen as the association of two (respectively, one) electron polarons and one fully ionized O vacancy. This allows to compute the association energy between the fully ionized O vacancy (V_O^{2+}) and two electron polarons ($2Fe_{Fe}^{'}$), as

$$\begin{aligned} E_{\text{assoc}}\left[V_O^{2+} - 2Fe_{Fe}^{'}\right] = {} & E_{\text{tot}}(\text{BFO} + V_O, 0) + 2E_{\text{tot}}(\text{BFO}) \\ & - E_{\text{tot}}(\text{BFO} + V_O, 2) \\ & - 2E_{\text{tot}}(\text{BFO}, -1), \end{aligned} \tag{6}$$

and the association energy between the singly ionized O vacancy (V_O^{1+}) and one electron polaron ($Fe_{Fe}^{'}$), as

$$\begin{aligned} E_{\text{assoc}}\left[V_O^{1+} - Fe_{Fe}^{'}\right] = {} & E_{\text{tot}}(\text{BFO} + V_O, 0) + E_{\text{tot}}(\text{BFO}) \\ & - E_{\text{tot}}(\text{BFO} + V_O, 1) \\ & - E_{\text{tot}}(\text{BFO}, -1), \end{aligned} \tag{7}$$

in which $E_{\text{tot}}(\text{BFO}, -1)$ is the energy of the supercell with the electron polaron. We find −0.81 and −0.47 eV for the association energy in Eqs. (6) and (7), respectively, indicating that the O vacancy strongly traps the two electrons released. Taking the band electron as reference, these trapping energies become −0.51 and −0.32 eV, giving the picture of a moderately deep donor.

However, this description of the polaron is strongly sensitive to the choice of U. Here, the used U, taken from Ref. [53], was chosen for its capability to reproduce correctly some bulk properties of BFO, not those of polarons. Larger values of U may contribute to stabilize the electron polaron. For polaronic systems, the most appropriate value of U may be determined by varying the polaronic charge between 0 and 1, as the one that best reproduces the theoretical piecewise linear behavior of the total energy as a function of fractional polaronic charge [65,66]. Such determination is presented in Appendix C, and leads to an ideal U of ∼5.5 eV. For such U value, the self-trapped electron polaron is finally found more stable than the band electron (computed with the atomic geometry of the perfect crystal), by −0.50 eV (this quantity is called hereafter the self-trapping energy). We note that electron polarons are stable in Fe_2O_3 [67], with, however, a moderate self-trapping energy of −0.23 eV.

B. Iron vacancy

The Fe vacancy is associated with three defect states lying in the band gap (Fig. 9).

1. Defect states

The iron vacancy is a triple acceptor defect. In its charge-neutral state, three empty states appear in the gap, with a well-defined spin (down in Fig. 9, the total spin of the defect is thus ±2 according to the sign of the spin of the Fe removed). The three defect states are denoted as *dn1*, *dn2*, and *dn3*. The density of probability of the lowest-energy of these three defect states (*dn1*) is shown in Fig. 10 (the two others have similar density of probability, localized on the same O atoms and the same $2p$ orbitals): they are localized on the O atoms surrounding the vacancy, mainly the three O atoms surrounded by a green circle in Fig. 3(b). This is related to the charge-transfer insulating nature of BFO, with a valence band top consisting mainly of oxygen $2p$ orbitals: the holes correspond to depopulated $2p$ states of oxygen. The three defect states can be seen as linear combinations of the three $2p$ oxygen orbitals oriented along the V_{Fe}^0-oxygen lines (the subspace spanned by these three orbitals forms the band of defect states). We have thus three oxygen-type spin-polarized hole polarons trapped in the vicinity of the Fe vacancy (the positive holes are attracted by the negative vacancy). It is noticeable that each hole is not localized on one oxygen but on three.

Upon charging negatively the defect, electrons come to occupy these states progressively. Once occupied, the states are stabilized and their energy decreases down to the VBM. When the vacancy is completely ionized (V_{Fe}^{3-}), the three states are against the VBM, as illustrated in Fig. 9.

Here comparison between GGA and LDA+U is interesting: in LDA+U, in charge state $q = -1$ and -2, the occupied levels do not separate from the band of defects states (the whole band is shifted towards the VBM), whereas in GGA, they do. This behavior is related to the probable better description of localized p states with GGA rather than with LDA (in the present LDA+U scheme, U is applied on Fe d but oxygen p orbitals are treated at the LDA level).

2. Electric dipole associated with the Fe vacancy

Whatever the charge state, the three defect states are localized on the three oxygen atoms of the octahedron surrounding the missing Fe and oriented in the direction of the polarization (these three O atoms are the ones that are the closest from the missing Fe owing to the FE distortion). It follows that, paradoxically, and although it is a *point* defect, *the isolated*

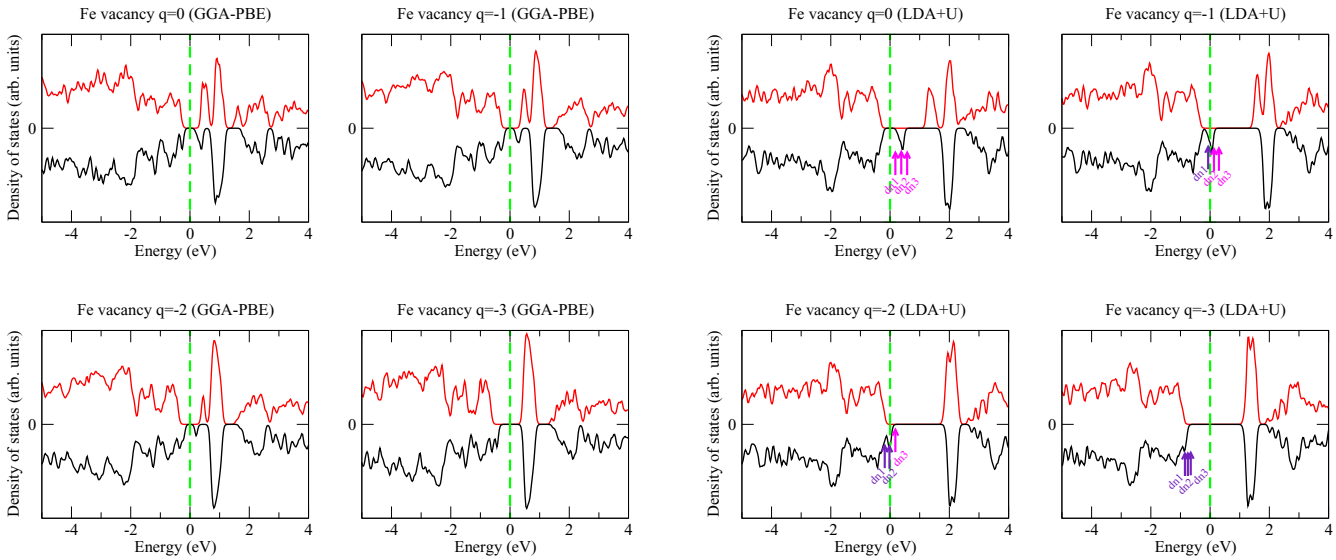

FIG. 9. e-DOS for the four charge states of the Fe vacancy. The zero of energy is placed approximately at mid-distance between the highest occupied and the lowest unoccupied state (dashed green vertical line). The arrows indicate where the defect states lie. The charge-neutral Fe vacancy (triple acceptor) generates three empty states of same spin lying in the band gap. Upon charging negatively the vacancy, these states become occupied and their energy decreases down to the top of the valence band. Positive/red curves: spin ↑, negative/black curves: spin ↓. Small violet (respectively, magenta) arrows: occupied (respectively, unoccupied) KS defect states.

charge-neutral Fe vacancy in BFO is associated with an electric dipole, oriented in the direction of the polarization: it may therefore cause an imprint effect. The charge-neutral Fe vacancy, V_{Fe}^{0}, is a pure dipole, and upon charging negatively the defect, it evolves from a pure dipole up to a pure charge, once it is fully ionized (V_{Fe}^{3-}).

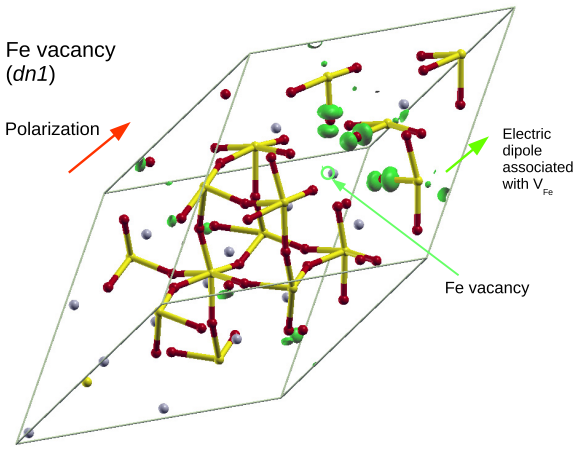

FIG. 10. Isosurface of the density of probability of the lowest-energy defect state associated to the iron vacancy (*dn1* on Fig. 9), in the neutral case ($q = 0$). The two other defect states have similar density of probability, localized on the same three oxygen atoms and the same $2p$ orbitals. The position of the Fe vacancy is shown with a green circle. This defect state (here empty) may be seen as associated to an oxygen-type hole localized on three O atoms first-neighbor of the missing Fe (this is also the case for the two other defect states). The three O atoms are the ones made the closest from Fe by the FE distortion [see Fig. 3(b)]. The defect carries therefore as its own an electric dipole, schematically shown by a green arrow. The straight grey lines are the edges of the 80-atom supercell.

Such behavior, which is related to the loss of symmetry of the defect environment caused by the FE distortion, should also be observed in the case of the oxygen vacancy. However, it is certainly not as strong, because the two electrons accompanying the neutral O vacancy are localized on the two sides of the O vacancy, although one of the two Fe is, indeed, closer from the missing O (owing to the FE distortion); moreover, concentrating two electrons on a single Fe atom would have a too large energy cost, and moreover, would not be compatible with the possible oxidation degrees of Fe. Only the O vacancy in charge state 1+ could exhibit similar dipolar behavior, as the Fe vacancy.

C. Bismuth vacancy

1. Metastable states

In the Bi vacancy case, we encountered a difficulty associated with the existence of metastable electronic states in spin-polarized DFT and DFT+U [68]: in a first series of LDA+U structural optimizations, we obtained, in that system, two of the charge states ($q = -1$ and -2) with defect states lying against the VBM, instead of being higher in the band gap. The corresponding densities of states are shown in Figs. 11(c) and 11(d) and are rather characteristic of a p-type metal. This was problematic because (i) the e-DOS obtained in the neutral case ($q = 0$) was qualitatively different (presence of defect states higher in the band gap), and (ii) the e-DOS obtained in GGA-PBE for these two charge states are also qualitatively different, exhibiting also defect states higher in the band gap. However, it appears that, in the $2 \times 2 \times 2$ supercell, the correct ground states are more easily obtained when applying also a Hubbard parameter U_p on the p orbitals of oxygen (see hereafter, Sec. VI B). Thus we used the final configurations obtained that way as inputs within the present LDA+U scheme ($U_p = 0$): this allowed to finally obtain electronic configurations which,

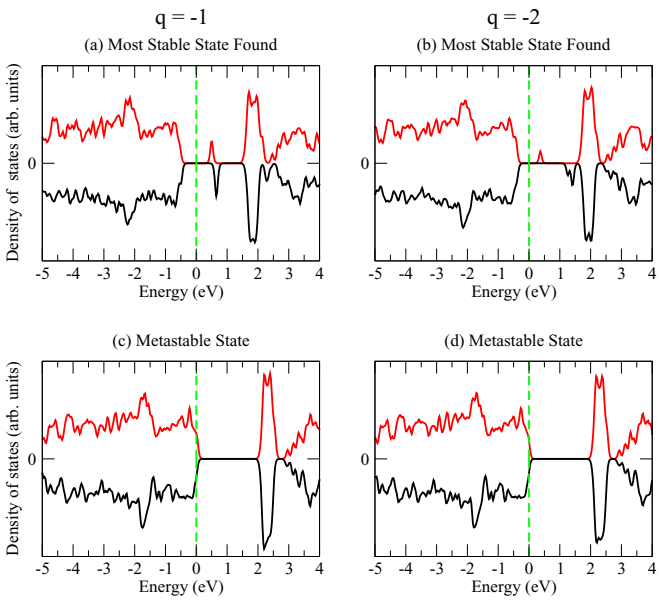

FIG. 11. e-DOS of the 80-atom BFO supercell with one Bi vacancy, as obtained in LDA+U. Left (respectively, right) Charge state 1− (respectively, 2−). (Top) The e-DOS for the configuration optimized with the electron gas in the most stable state that we found. (Bottom) The e-DOS for the configuration optimized with the electron gas in a metastable state. The green dashed line separates occupied from unoccupied states. Positive/red curves: spin ↑, negative/black curves: spin ↓.

after structural optimization, are more stable than the two initially found (by ∼0.43 and 0.13 eV, respectively), and qualitatively similar to the neutral case and to the GGA ones, i.e., exhibiting clearly KS defect states rather high in the band gap. Their e-DOS are displayed in Figs. 11(a) and 11(b). It is important to point out the possibility of metastable states in DFT+U in the calculation of this spin-polarized defect.

2. *Defect states*

The Bi vacancy is, as the Fe vacancy, a triple acceptor defect. It is associated with defect states lying in the band gap (Fig. 12). We first focus on the charge-neutral vacancy V_{Bi}^{0}. Three empty $2p$ oxygen-type states appear in the gap, two of them with a given spin (denoted as *up1* and *up2* in Fig. 12) and lying rather high in the gap (∼1 eV), and another one, with opposite spin, at the edge of the VBM (denoted as *dn1* in Fig. 12). Moreover, another band of empty states, with also opposite spin, is present, consisting of three $3d$-type states localized on one Fe atom (denoted as *dn2*, *dn3*, and *dn4* in Fig. 12). This makes, surprisingly, six states in the band gap associated with the presence of the defect.

In contrast to the O and Fe vacancies, these KS states are not localized close to the Bi vacancy, they lie a bit farther away in the supercell. More precisely, the three oxygen-type states lie on six oxygen atoms [visible in Fig. 13(a), in the case of V_{Bi}^{1-}]. They originate from the depopulating of states at the VBM. The two highest-energy oxygen-type states (*up1*, *up2*), in particular, are mostly on three oxygen atoms forming the half of an octahedron cage [we denote these three oxygen atoms as O_{A1}, O_{A2}, and O_{A3}, see Fig. 13(b)]. It follows that three Fe-O bonds in this octahedron are weakened, and the Madelung potential on the central Fe is lowered (note that its spin state is also drastically changed, with a spin magnetic moment of ∼2.5 μ_B). As a consequence, three $3d$ unoccupied states of this Fe leave the CB and go down in the gap, forming the defect band with Fe $3d$ character and spin down, marked with orange arrows in Fig. 12 (states *dn2*, *dn3*, and *dn4*). The third oxygen-type state, *dn1*, mostly lies on the other three oxygen atoms, denoted as O_{B1}, O_{B2}, and O_{B3}, located between the previous oxygens and the Bi vacancy [see Fig. 13(b)]. This localization of the defect states beyond the first coordination shell of the vacancy may be related to an elastic effect; indeed, among the three charge-neutral defects here studied, the Bi vacancy is the one that generates the largest (negative) pressure in the supercell, and possesses the largest elastic dipole tensor (see hereafter Sec. V). Other examples of that kind do exist in oxides: Lindman *et al.* have shown that the hole polaron associated with the Y (acceptor) dopant in $BaZrO_3$ is localized, in its most stable state, on the oxygen second neighbor [66]. Moreover, we have recently shown, in the case of acceptor-doped $BaSnO_3$, that this was clearly related to a dopant size (and thus elastic) effect, this specific localization occurring for the largest dopants only [69]. We note that the position (in the bandgap) of the Bi vacancy defect states is in agreement with that of Paudel *et al.*, [18] but qualitatively differs from the one given by Shimada *et al.* [40], since the latter HSE06 calculations provide only three defect states, lying much closer to the VBM.

In the 1− charge state, the lowest-energy oxygen-type defect state (*dn1*), which is against the VBM in the neutral case, becomes occupied, leaving only two empty oxygen-type defect states (*up1*, *up2*), which still lie rather high in the band gap [Fig. 13(a)]. The three Fe-$3d$-like states (*dn2*, *dn3*, and *dn4*) are still at the same place in the band gap, localized on a Fe atom with spin magnetic moment still ∼2.5 μ_B.

In the 2− charge state, only one of these oxygen-type defect states remains empty, the other, once occupied, comes against the VBM, while *dn1* is slightly below the VBM. The Fe-$3d$-like states (*dn2*, *dn3*, and *dn4*) have their energy increased: the Fe atom on which they are localized has now a magnetic moment of 3.3 μ_B.

Finally, when the vacancy is completely ionized ($q = -3$), the oxygen-type states lie all three against or inside the VB [Fig. 13(b)]: two of them (*up1* and *up2*) clearly keep a spatially localized character and are just at the VBM, while the third one (*dn1*) falls in the VB, ∼at 0.2–0.3 eV below the VBM: it appears thus as hybridized with valence band states and is more delocalized. According to the total charge of the defect (from $q = 0$ to -3), these oxygen-type defect states evolve from empty to occupied and have their energy progressively lowered, until they lie next to the top of the valence band (or just below). At the same time, the Fe $3d$ defect states are more and more destabilized and eventually join the CB when the vacancy is completely ionized.

V. ELASTIC EFFECTS OF VACANCIES

In this part, we examine the elastic effects of charge-neutral vacancies, i.e., whether their presence tends to produce an expansion or a contraction of the crystal, which can be done

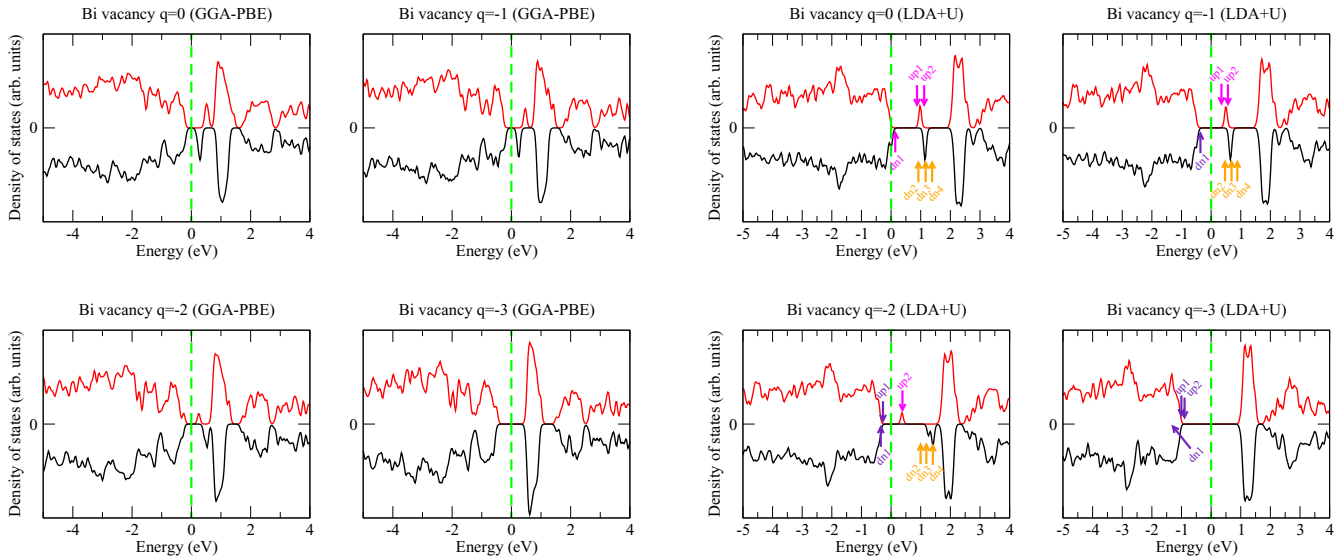

FIG. 12. e-DOS for the four charge states of the Bi vacancy. The zero of energy is placed approximately at mid distance between the highest occupied and the lowest unoccupied state (dashed green vertical line). The arrows indicate where the defect states lie. Positive/red curves: spin ↑, negative/black curves: spin ↓. Small violet (respectively, magenta) arrows: occupied (respectively, unoccupied) KS defect states. Small orange arrows: unoccupied Fe-3*d* KS states in the band gap.

by computing the so-called *elastic dipole tensor*, associated to each kind of defect [70–73]. Following Ref. [73], the energy of a simulation box (with volume V) containing one defect, in which all atomic positions are relaxed, and subject to a homogeneous strain $\{\epsilon_{ij}\}$ (defined by taking as reference the perfect rhombohedral lattice) may be written as

$$E(\{\epsilon_{ij}\}) = E_0 + E_D + \frac{V}{2}\sum_{ijkl} C^{\rm rh}_{ijkl}\epsilon_{ij}\epsilon_{kl} - \sum_{ij}\epsilon_{ij}G^{\rm eff}_{ij}, \quad (8)$$

in which E_0, E_D, and $C^{\rm rh}_{ijkl}$ are, respectively, the bulk reference energy, the (unstrained) defect formation energy, and the elastic constants of the bulk rhombohedral compound. Here we refer to an *effective* elastic dipole tensor, denoted as $G^{\rm eff}_{ij}$, because in a multiferroic crystal, the elastic effect associated with a point defect can be impacted by the coupling of the strain with the internal degrees of freedom such as polarization (electrostriction), oxygen octahedra rotations

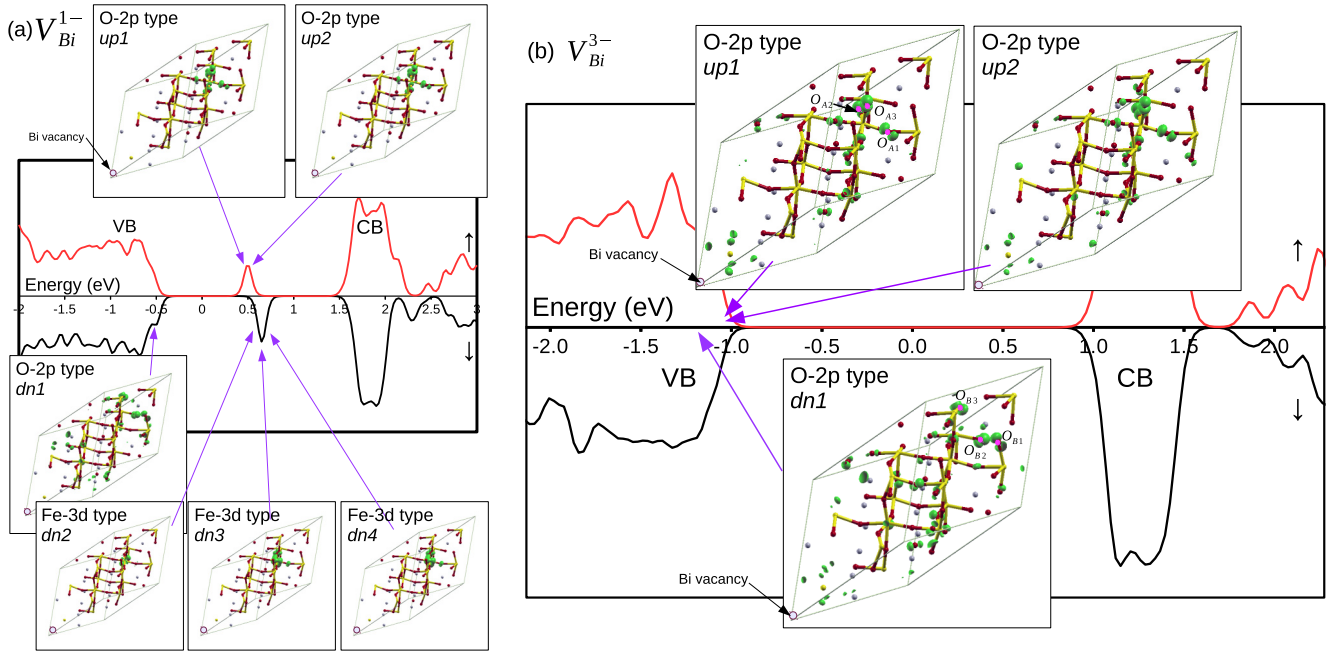

FIG. 13. e-DOS for (a) the partially ionized Bi vacancy ($q = -1$), and (b) the fully ionized Bi vacancy ($q = -3$). Positive/red curves: spin ↑, negative/black curves: spin ↓. An isosurface of the associated defect states is shown in both cases. The zero of energy is set approximately at mid-distance between the highest-occupied and the lowest-unoccupied KS levels. The straight grey lines are the edges of the 80-atom supercell. Note that, due to periodic boundary conditions, periodic images of the Bi vacancy lie at all the corners of the supercell.

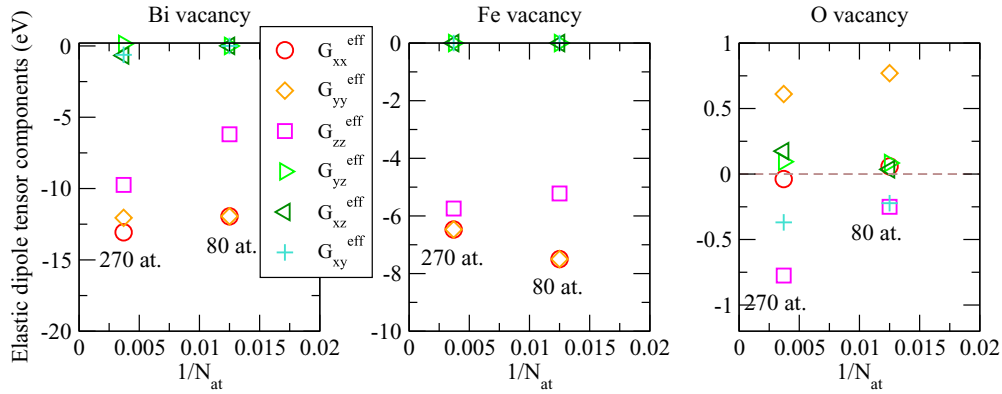

FIG. 14. (Effective) elastic dipole tensor components (eV) vs the inverse of the number of atoms N_{at} in the perfect supercell, for the charge-neutral Bi, Fe, and O vacancies. z corresponds to the polar axis of the crystal ([111] direction in terms of pseudocubic axis).

(rotostriction), and magnetism (magnetostriction) [74]. The stress tensor is the positive derivative of the energy with respect to strain, which yields

$$\sigma_{ij} = \frac{1}{V}\frac{\partial E}{\partial \epsilon_{ij}} = \sum_{kl} C^{\text{rh}}_{ijkl}\epsilon_{kl} - \frac{1}{V}G^{\text{eff}}_{ij}. \tag{9}$$

Under fixed strain $\epsilon_{kl} = 0$, we simply get $G^{\text{eff}}_{ij} = -V\sigma_{ij}$. Therefore G^{eff}_{ij} can be obtained from the stress *induced by the presence of the vacancy* in a supercell in which all the atomic positions are relaxed, but the lattice vectors are kept fixed to those of the perfect rhombohedral BFO lattice. As indicated in Ref. [70], a positive (respectively, negative) diagonal component G^{eff}_{ii} of this tensor means that the defect tends to expand (respectively, contract) the crystal along the Cartesian direction i.

Practically, G^{eff} is computed from the stress tensors obtained in the $2 \times 2 \times 2$ and $3 \times 3 \times 3$ supercells containing one vacancy (with atomic positions optimized, but supercell vectors kept fixed to those of the perfect crystal). This computation is restricted to the charge-neutral defects [75]. For the sake of numerical precision, the total energy and stress of the optimized configurations described previously are recomputed using denser k-point meshes: $3 \times 3 \times 3$ (respectively, $2 \times 2 \times 2$) in the case of the $2 \times 2 \times 2$ (respectively, $3 \times 3 \times 3$) supercell. The elastic dipole tensor components are plotted in Fig. 14, for each defect, as a function of inverse number of atoms in the perfect supercell.

It follows that the charge-neutral Bi and Fe vacancies tend to contract the lattice, the largest contraction being associated with V_{Bi}. The contraction is more pronounced in the directions perpendicular to the polarization axis. In contrast, the neutral O vacancy has a weaker, but very anisotropic elastic effect: it tends to contract the lattice along the polar axis of the crystal and rather expands it in one direction perpendicular to it.

It should be noted that the elastic dipole tensor components along the two directions perpendicular to the polar axis (z) are expected to be equal in the case of the Bi and Fe vacancies: $G^{\text{eff}}_{xx} = G^{\text{eff}}_{yy}$. This is indeed the case except for the Bi vacancy computed in the $3 \times 3 \times 3$ supercell. Indeed, in the latter calculation, a metastable state of the Bi vacancy was probably reached instead of the ground state (see Appendix A).

VI. DISCUSSION

A. Electrons and electron polarons in bismuth ferrite

We have seen that the self-trapped electron polaron is localized on an iron atom (which formally becomes Fe^{2+}), and is associated with a self-trapping distortion around it, with the distances to nearest-neighbor oxygens being enhanced [Fig. 15(a)]. The state occupied by the extra electron is ~0.3 eV below the CBM [Fig. 15(b)], using $U = 3.87$ eV. However, as explained above, this electron polaron appears as not stable using LDA+U with $U = 3.87$ eV, but calculations using $U = 5.5$ eV (the value of U that provides, for the energy of the polaronic configuration as a function of fractional polaronic charge, a behavior close to the piecewise linearity) suggest that electrons may localize as self-trapped polarons in BFO, with a self-trapping energy of −0.5 eV. In our simple defect model—based on formation energies obtained with $U = 3.87$ eV—this entity was not taken into account. It is clear, however, that electron polarons may be present in significant concentration, as resulting from the ionization of oxygen vacancies (which are often invoked as being at the root of the leakage currents observed in BFO films). In order to estimate their effect, we artificially introduce the electron polaron, with a formation energy equal to $E_g + E_{\text{st}} - \epsilon_F$, as a defect in Eq. (3) (with $E_{\text{st}} = -0.5$ eV being the electron polaron self-trapping energy). In oxidative conditions, the estimations of Sec. III A are not modified, with holes dominating over electrons and electron polarons. In reducing ones, however, the equilibrium Fermi level is decreased to 1.02 eV (versus 1.30 eV without the polaron), with the electron polaron concentration being as large as that of free holes: $n^{\text{pol}} \approx p$ (both charge carriers remain however in much lower concentration than in oxidative conditions).

B. Holes and hole polarons in bismuth ferrite

1. Self-trapped holes and itinerant holes

As suggested in previous sections and previous *ab initio* studies, defects (in particular the ionized bismuth vacancy) in BFO mostly induce p-doping, releasing holes. How those released holes will contribute to conductivity will depend on whether they localize away from defects in the form of self-trapped small polarons, or remain of the valence band

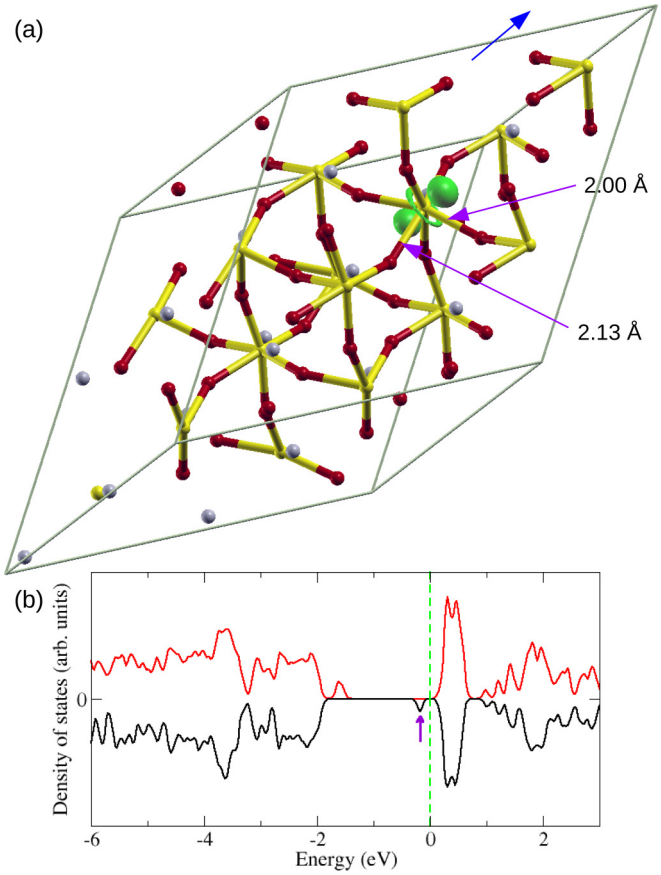

FIG. 15. (a) Isosurface of the KS state occupied by the self-trapped electron polaron in BFO (as obtained from LDA+U with $U = 3.87$ eV). The electron is localized on a single Fe atom (which is formally reduced to the Fe^{2+} state), and occupies a state with marked Fe $3d$ character. The figure also displays the atomic geometry around it, with the self-trapping distortion visible (the distance of Fe to nearest oxygens is enhanced to 2.00 and 2.13 Å vs 1.94 and 2.07 Å in bulk). The blue arrow indicates the direction of polarization. (b) e-DOS of the BFO supercell with the self-trapped electron polaron ($U = 3.87$ eV). The KS state occupied by the electron polaron is spotted with a violet arrow.

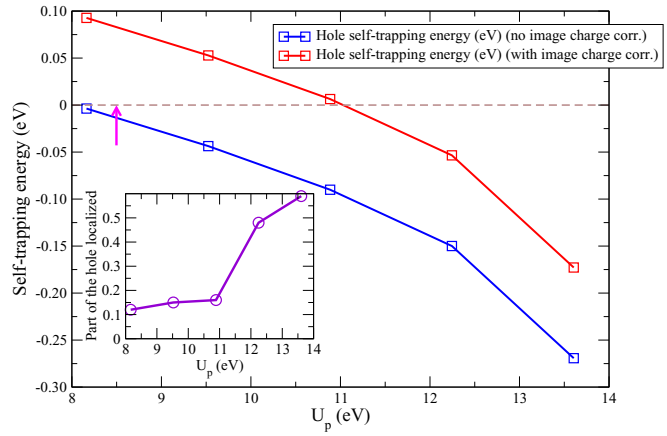

FIG. 16. Hole polaron self-trapping energy (eV) as a function of Hubbard parameter U_p applied on oxygen p orbitals (with $U = 3.87$ eV on Fe d orbitals). The arrow indicates the value of U_p for which the energy as a function of fractional polaronic charge is close to piecewise linearity (see Appendix C). (Inset) Part of the hole charge which is localized on a single oxygen atom.

Bloch state nature. Those holes will be made of a combination of oxygen $2p$ orbitals in the latter case, while they will be localized on a single $2p$ orbital in the case of small hole polarons.

Unfortunately, these oxygen-type self-trapped hole polarons (if any) cannot be described by using standard local and semilocal XC functionals (LDA, GGA), a problem traditionnally attributed to the self-interaction error that is inherent to these functionals. Hybrid functionals containing Hartree-Fock exchange (PBE0, HSE06) in contrast, are able to correctly reproduce these entities. Nevertheless, and more conveniently, it has been shown in a number of recent works that DFT+U, with U applied on the p states of oxygen, provides a satisfactory compromise between accuracy and computational cost to describe these hole polarons [65]. Using such technique, oxygen-type self-trapped hole polarons have been shown to be more stable than band holes in several perovskite oxides, such as $BaTiO_3$, $SrTiO_3$ [65], $BaZrO_3$ [66], or $BaSnO_3$ [69]. In constrast, they are not stable in $PbTiO_3$ [30,65].

In the present work, U has been applied only on the d states of iron so far. It means that oxygen-type self-trapped hole polarons, if they exist, cannot be accessed by our numerical method: with LDA or GGA, we only capture oxygen-type hole polarons, which are *trapped* by a defect (e.g., here cationic vacancy, see above), but *not in their self-trapped* state (i.e., the hole polarons in the lattice).

In order to determine if released holes may localize as small polarons, or remain delocalized Bloch-like states, we thus added a supplemental U in our calculations (let us denote it as U_p), which we applied on the p states of oxygen. Within this LDA+U + U_p scheme, we first construct a polaronic configuration using a large value of U_p. Practically, this is done, as for the electron polaron, by removing one electron from the undefective supercell, forcing the localization of this hole on one single oxygen atom, and structurally optimizing the system. The polaronic configuration so obtained is then used to determine the best possible value of U_p, as the one for which the energy as a function of fractional polaronic hole charge is the closest from piecewise linearity. This calculation is presented in Appendix C, and leads to $U_p \sim 8.5$ eV. For different values of U_p, we also optimize the polaronic configuration containing the self-trapped hole, and compute the energy of the band hole (in the undistorted crystal reoptimized with the considered U_p): the energy difference between the self-trapped polaronic configuration and the band hole is the hole self-trapping energy, which is plotted in Fig. 16 as a function of U_p. For $U_p \sim 8.5$ eV, we see that the self-trapping energy is between ~ -0.02 and $+0.08$ eV (whether the image-charge correction is accounted for or not for the polaron), suggesting that self-trapped hole polarons in BFO are probably, either not stable, or having stability close to that of band holes. We note that for $U_p = 8.5$ eV, only $\sim$10%–15% of the hole charge is localized on a single oxygen atom (the other 85%–90% being delocalized on all the other oxygens of the supercell, see Fig. 16 (inset)), which is much

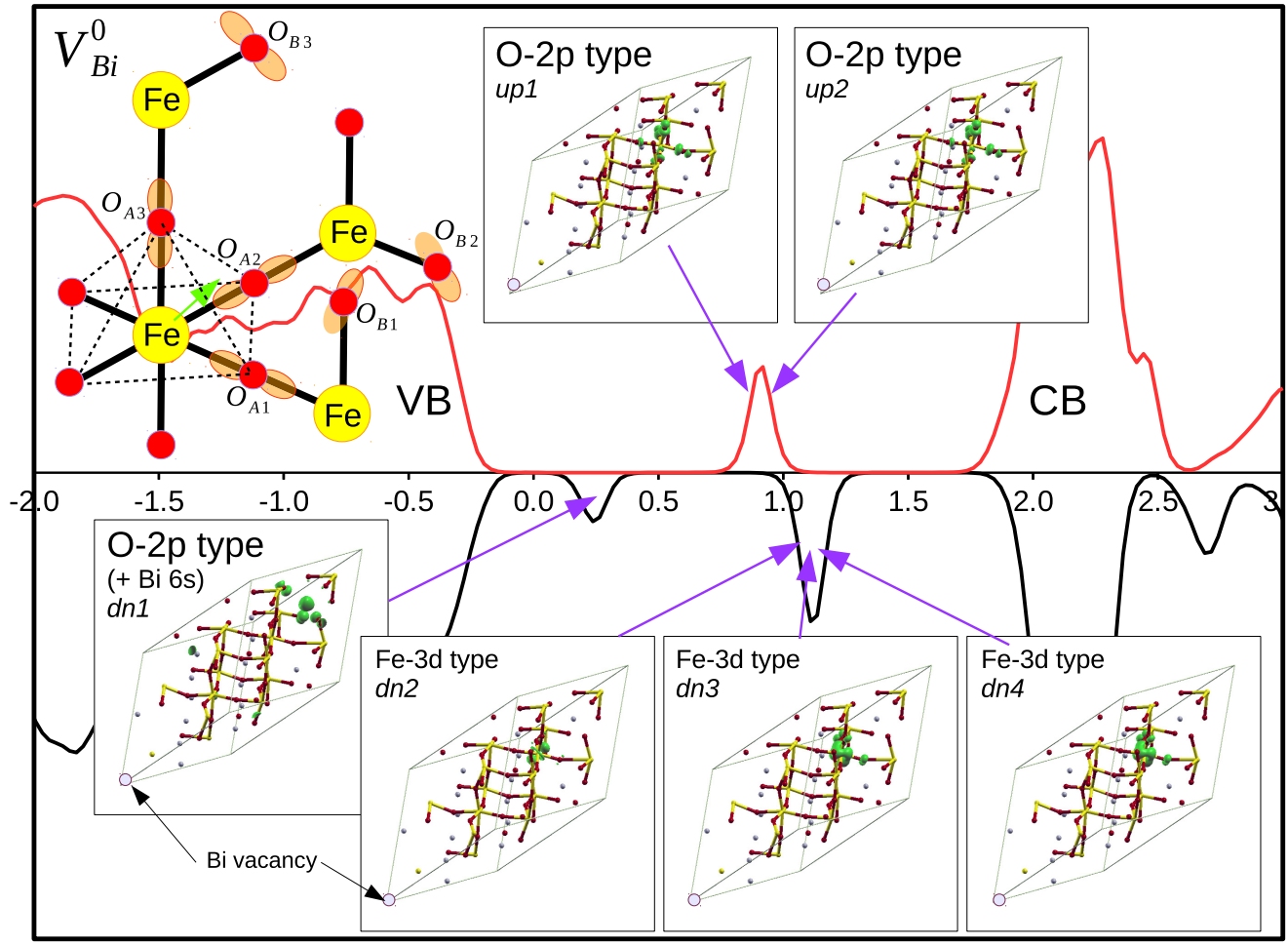

FIG. 17. e-DOS for the charge-neutral Bi vacancy as obtained with LDA+U + U_p, i.e., Hubbard term applied on oxygen p ($U_p = 8.5$ eV), and on Fe d ($U = 3.87$ eV). The zero of energy (0 eV) is placed approximately at mid-distance between the highest occupied and the lowest unoccupied KS state. Positive/red curves: spin ↑, negative/black curves: spin ↓. An isosurface of the density of probability of the KS states associated with the defect (in the band gap) is shown. The picture in the top left corner schematically represents the six oxygen atoms and the six $2p$ orbitals that receive the holes released by the Bi vacancy (which is located one unit cell further along the [111] direction). The straight grey lines are the edges of the 80-atom supercell.

less than, e.g., for the hole polaron in $BaSnO_3$ [69], suggesting that, indeed, the hole is close to being delocalized, even under the polaronic form.

2. *Holes trapped by cationic vacancies*

LDA+U + U_p (with $U_p = 8.5$ eV on oxygen p orbitals, and $U = 3.87$ eV on Fe d orbitals) was then used to recompute the supercell with the Bi and Fe vacancies, in their different charge states. Figure 17 displays the e-DOS obtained in the case of the charge-neutral Bi vacancy. Qualitatively, this DOS, as well as the defect states density of probability, are similar to the one obtained without U_p (Fig. 12), at the exception that the lowest-energy defect state ($dn1$), which lies at the edge of the VB without U_p, now clearly lies higher in the band gap (see Fig. 17). This state is localized on three $2p$ orbitals of three oxygen atoms (and also on a Bi $6s$). Although the calculation is performed without symmetry constraints, the state is not found as localized on a single atom, here again, but mostly on three. This is also the case for the two spin-up oxygen-type defect states of Fig. 17 ($up1$, $up2$). This numerical scheme clearly describes better localized oxygen p states. Note that GGA-PBE provides qualitatively the same kind of description: the charge-neutral Bi vacancy in GGA is found to have its defect states localized high in the band gap (see Fig. 12).

C. Possible intrinsic causes of imprint in $BiFeO_3$

We have identified two possible intrinsic sources of polar imprint in BFO. The first one is related to the clustering of cationic and oxygen vacancies, which have the tendency to associate, forming dipoles with some preferential directions. The driving force for cationic and oxygen vacancies association is the electrostatic charge-charge interaction, which is the most favorable for the smallest cation-oxygen distance, rather than the interplay with the polarization: the most stable configurations for these divacancies are those for which the distance

between the (missing) cation and oxygen is the smallest. Since these short distances are the consequence of the FE distortion, they are also the configurations in which the divacancy dipole forms the smallest angle with the polarization. This can be seen explicitly on the $[\text{Bi-O}]_2$ and $[\text{Bi-O}]_3$ configurations: both exhibit the same angle between the bidefect dipole and the polarization, $\sim 100^\circ$, but the Bi-O distance is much larger in $[\text{Bi-O}]_3$ (3.31 Å versus 2.48 Å for $[\text{Bi-O}]_2$), which is less stable than $[\text{Bi-O}]_2$.

The second one is related to Fe single vacancies, which, in their neutral or partially ionized states, locate holes on the three closest oxygens, and not on all six anions forming the oxygen octahedral cage. As a result, the Fe vacancy generates its own local dipole, parallel and in the same direction as the polarization.

VII. CONCLUSION

In this work, we have accurately described cationic and oxygen vacancies in bismuth ferrite, as well as the related electronic defect states. We now summarize the main results.

(1) In agreement with several previous works [18,19,37], BFO is found to possibly exhibit p-type conduction in oxygen-rich conditions, probably mediated by delocalized band holes rather than hole polarons. These holes are released by the cationic vacancies (mostly the Bi ones), for which the transition energy levels (found typically $\leqslant$ 0.5–0.6 eV above the VBM) may be rather easily ionized in such atmospheres.

(2) In oxygen-poor conditions, our simple defect model suggests that BFO tends to recover a regime with a concentration of electronic free carriers much lower than in oxygen-rich conditions.

(3) Cationic and oxygen vacancies have the tendency to associate in configurations for which the cation-oxygen distance is as short as possible. Owing to the strong FE distortion in BFO, these configurations are also those for which the as-formed defect dipole makes the smallest angle with the polarization, leading to possible imprint effects.

(4) These bidefects, moreover, have transition energy levels closer to the band edges than the corresponding isolated defects, indicating that the defects might be more easily ionized in such configurations than isolated. This may be explained by the large gain of (electrostatic) association energy obtained when the two defects are ionized.

(5) All monovacancies exhibit, in their neutral state, defect states in the band gap. Upon progressive ionization, the defect states are joining the VBM or the CBM, whether the ionization corresponds to filling or emptying the states. Figure 18 illustrates schematically how the energies of the defect states evolve with the charge state of the defect in LDA+U.

(6) The O vacancy is a double, moderately deep, donor. In its charge-neutral state, the two associated electrons are trapped close to the vacancy on the two first-neighbor Fe atoms, which therefore are reduced formally into Fe^{2+}. Each electron occupies a Fe 3d state.

(7) LDA+U with U (on Fe d orbitals) determined according to piecewise linearity of the energy as a function of fractional polaronic charge ($U = 5.5$ eV with LDA), leads to a self-trapped electron polaron (occupying a Fe 3d orbital with spin opposite to that of this Fe atom) more stable than the delocalized electron. $U = 3.87$ eV leads, in contrast, to an electron polaron, which is metastable with respect to the delocalized electron.

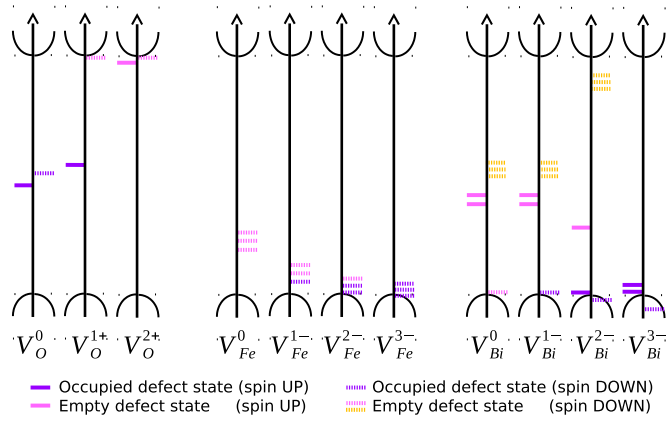

FIG. 18. Schematic evolution of the KS quantum eigenstates associated with the defect in the case of the O, Fe, and Bi vacancies, from the neutral to the completely ionized defect.

(8) The Fe vacancy is a triple, moderately deep, acceptor. In its neutral state, the three holes released are trapped close to the vacancy on the 2p orbitals of three oxygen atoms. The vacancy and the three holes form a dipole oriented in the direction of the polarization, which is a possible source of imprint.

(9) The Bi vacancy is associated with several metastable electronic states. In the most stable one found, it is a triple, moderately deep, acceptor. In its neutral state, it carries three holes, localized on the 2p orbitals of oxygen atoms which do not belong to the first coordination shell of the missing Bi. This might be related to an elastic effect. These oxygen-type holes weaken the Madelung potential on a particular Fe atom, and thus, three Fe 3d empty states leave the CB and go down in the gap, resulting in a change of the spin magnetic moment of this Fe atom: 2.5 (respectively, 3.3) μ_B when there are two holes (respectively, one hole) localized around it, versus 4 μ_B on other unperturbed Fe atoms.

(10) Holes, once they have escaped from their parent defect, are probably delocalized in Bloch-like states rather than as oxygen-type hole polarons.

(11) Charge-neutral Bi and Fe vacancies tend to contract the lattice, while the charge-neutral O vacancy has a very anisotropic elastic effect.

APPENDIX A: CALCULATIONS USING A 270-ATOM SUPERCELL

The formation energies of the O, Bi, Fe, and $[\text{Bi-O}]_1$ vacancies have been recomputed using a large $3 \times 3 \times 3$ supercell of BFO (this corresponds to 270 atoms in the perfect system). Results are gathered in Table V. It may be seen that the formation energies obtained for the O and Fe vacancies in the large supercell are very close to those obtained in the smaller one (maximal difference 0.15 eV). Moreover, the e-DOS obtained for the O vacancy in the large supercell (Fig. 19) are similar to the ones obtained in the smaller one. This suggests that the 80-atom supercell, which has been used

TABLE V. Formation energies (in eV) of the oxygen, bismuth, and oxygen-bismuth pair ($[\text{Bi-O}]_1$) vacancies at the VBM ($\epsilon_F = 0$), for $\Delta\mu_O = -2.0$ eV, $\Delta\mu_{Bi} = -0.94$ eV, and $\Delta\mu_{Fe} = -2.04$ eV, calculated using $2 \times 2 \times 2$ and $3 \times 3 \times 3$ supercells.

Formation energies ΔE_f	$2 \times 2 \times 2$	$3 \times 3 \times 3$
V_O^{2+}	−0.52	−0.67
V_O^{1+}	0.79	0.74
V_O^{0}	2.36	2.39
$V_{[\text{Bi-O}]_1}^{2+}$	2.93	2.95
$V_{[\text{Bi-O}]_1}^{1+}$	2.97	2.90
$V_{[\text{Bi-O}]_1}^{0}$	3.21	3.20
$V_{[\text{Bi-O}]_1}^{1-}$	3.60	3.64
$V_{[\text{Bi-O}]_1}^{2-}$	5.37	5.52
$V_{[\text{Bi-O}]_1}^{3-}$	7.52	7.32
V_{Bi}^{0}	4.18	4.55[a]
V_{Bi}^{1-}	4.33	4.65[a]
V_{Bi}^{2-}	4.90	5.00[a]
V_{Bi}^{3-}	5.39	5.39
V_{Fe}^{0}	4.31	4.31
V_{Fe}^{1-}	4.87	4.76
V_{Fe}^{2-}	5.38	5.33
V_{Fe}^{3-}	5.95	6.02

[a]probable metastable state.

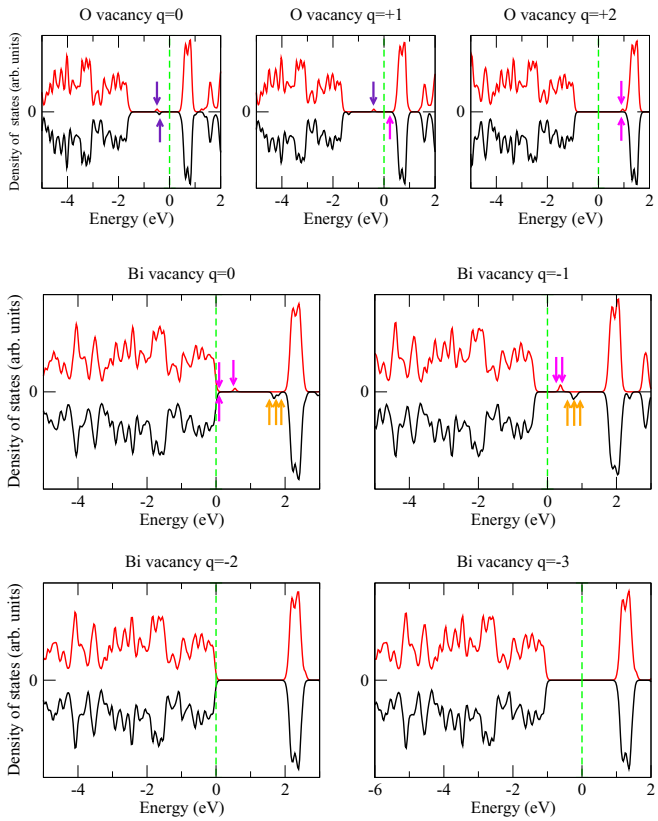

FIG. 19. e-DOS obtained for the O and Bi vacancies in a $3 \times 3 \times 3$ supercell.

throughout this work, provides very correct estimations for the defect formation energies. The formation energies obtained with the two supercells are also very close to each other in the case of the $[\text{Bi-O}]_1$ vacancy, except for $V_{[\text{Bi-O}]_1}^{3-}$ where the difference reaches 0.20 eV.

For the neutral and singly ionized state of V_{Bi}, however, the formation energy is found much larger in the large supercell than in the smaller one (by 0.37 and 0.32 eV, respectively), whereas the fully ionized Bi vacancy has the same formation energy in both cases. This suggests that, here again, the calculation in the large supercell has only reached metastable states. This is confirmed by examining the densities of states for the different charge states (Fig. 19), which do not look as being in coherence with each other (in contrast to what is obtained in the 80-atom supercell): the e-DOS of V_{Bi}^{0} differs from the one obtained in the smaller supercell by the state *up1* being at the VBM instead of higher in the gap. Upon charging (V_{Bi}^{1-}), a state close to that obtained in the 80-atom supercell is recovered, with *up1* and *up2* being high in the gap, with, however, the noticeable exception that the holes are not localized on the same oxygen atoms. Finally, the e-DOS of V_{Bi}^{2-} looks similar to that of the metastable state described in Sec. IV C 1.

APPENDIX B: COMPUTATION OF THE SELF-TRAPPED ELECTRON POLARON

The self-trapped electron polaron alone in the supercell has been obtained using the two-step methodology described in Ref. [69], which allows to simulate the self-trapped polaron on the chosen atom, and in the chosen orbital.

(1) First, a structural optimization is performed under the constraint of the extra charge being localized on the chosen atom and in the chosen orbital. Practically, this is achieved, with the ABINIT code, by using the possibility to constrain over a certain number of electronic steps the occupation matrices of the correlated orbitals within DFT+U (those on which U is applied). Here, the constraint is maintained over all the electronic steps of each ionic step [76]. The aim of this first step is to create around the polaron the self-trapping distortion favorable to its localization. It does not need to be pushed to very low atomic forces.

(2) Then, in a second step, the structural optimization restarts from the last configuration obtained at the first step, but the previous constraint is applied only on a few electronic steps of the first ionic step, and then is completely released. The system then terminates to structurally optimize, with the polaron localized on the chosen atom, and in the chosen orbital, except, of course, if such localization appears to be unstable.

(3) Here, the five possibilities for the d orbitals have been tested, but finally, all five calculations have led to the same final configuration, with the electron polaron localized on one Fe, in the same orbital. An isosurface of this occupied state is plotted in Fig. 15(a).

APPENDIX C: DETERMINATION OF U TO DESCRIBE THE SELF-TRAPPED POLARONS IN BFO

Figure 20(a) displays the energy change with respect to piecewise linearity as a function of the fractional number

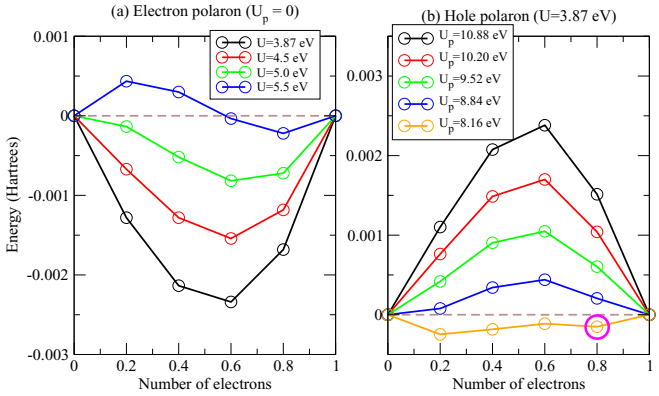

FIG. 20. Energy change with respect to piecewise linearity as a function of the fractional number of electrons in a supercell containing a self-trapped electronic polaron (left) or a self-trapped hole polaron (right) in BFO. In the first case, different U are applied on Fe d orbitals (within LDA+U), without U_p applied on oxygen p. In the second case, $U = 3.87$ eV is fixed on Fe d orbitals, and different U_p are applied on oxygen p orbitals (LDA+U + U_p).

of electrons [77], for different U applied on Fe d orbitals (within LDA+U), in a (frozen) configuration containing an electron polaron (the electron polaron corresponds to a number of 1 electron). Varying the charge of the supercell between 0 and 1 corresponds also to varying the charge in the polaron. The U that allows to have the smallest deviation from piecewise linearity is close to 5.5 eV. We insist on the fact that this calculation is done on a *polaronic* configuration.

Similarly, Fig. 20(b) displays the energy change with respect to piecewise linearity as a function of fractional number of electrons, for different U_p applied on oxygen p orbitals (within LDA+U + U_p), in a (frozen) configuration containing a hole polaron (the hole polaron corresponds to a number of 0 electron), with U on Fe d orbitals fixed to 3.87 eV. The U_p that allows to have the smallest deviation from piecewise linearity is close to 8.5 eV. Note that this value of U_p may be strongly sensitive to the radius of the oxygen PAW dataset (here 1.4 a.u.). Also, at the lowest U_p (8.16 eV), one point (the one surrounded in magenta in Fig. 20(b), which corresponds to a supercell charge of 0.2) does not follow the expected trend: indeed, in contrast to other calculated points, the hole polaron is completely lost in this case, the additional positive charge (0.2 in terms of elementary charge) is completely delocalized.

[1] G. Catalan and J. F. Scott, Adv. Mater. **21**, 2463 (2009).
[2] R. Palai, R. S. Katiyar, H. Schmid, P. Tissot, S. J. Clark, J. Robertson, S. A. T. Redfern, G. Catalan, and J. F. Scott, Phys. Rev. B **77**, 014110 (2008).
[3] F. Gao, Y. Yuan, K. F. Wang, X. Y. Chen, F. Chen, J.-M. Liu, and Z. F. Ren, Appl. Phys. Lett. **89**, 102506 (2006).
[4] J. F. Ihlefeld, N. J. Podraza, Z. K. Liu, R. C. Rai, X. Xu, T. Heeg, Y. B. Chen, J. Li, R. W. Collins, J. L. Musfeldt, X. Q. Pan, J. Schubert, R. Ramesh, and D. G. Schlom, Appl. Phys. Lett. **92**, 142908 (2008).
[5] S. R. Basu, L. W. Martin, Y. H. Chu, M. Gajek, R. Ramesh, R. C. Rai, X. Xu, and J. L. Musfeldt, Appl. Phys. Lett. **92**, 091905 (2008).
[6] A. Kumar, R. C. Rai, N. J. Podraza, S. Denev, M. Ramirez, Y.-H. Chu, L. W. Martin, J. Ihlefeld, T. Heeg, J. Schubert, D. G. Schlom, J. Orenstein, R. Ramesh, R. W. Collins, J. L. Musfeldt, and V. Gopalan, Appl. Phys. Lett. **92**, 121915 (2008).
[7] C. Paillard, X. Bai, I. C. Infante, M. Guennou, G. Geneste, M. Alexe, J. Kreisel, and B. Dkhil, Adv. Mater. **28**, 5153 (2016).
[8] C. Paillard, B. Xu, B. Dkhil, G. Geneste, and L. Bellaiche, Phys. Rev. Lett. **116**, 247401 (2016).
[9] Y. P. Wang, L. Zhou, M. F. Zhang, X. Y. Chen, J.-M. Liu, and Z. G. Liu, Appl. Phys. Lett. **84**, 1731 (2004).
[10] X. Qi, J. Dho, R. Tomov, M. G. Blamire, and J. L. MacManus-Driscoll, Appl. Phys. Lett. **86**, 062903 (2005).
[11] S. K. Singh, H. Ishiwara, and K. Maruyama, J. Appl. Phys. **100**, 064102 (2006).
[12] S. K. Singh, H. Ishiwara, and K. Maruyama, Appl. Phys. Lett. **88**, 262908 (2006).
[13] P. Pipinys, A. Rimeika, and V. Lapeika, Ferroelectrics **396**, 60 (2010).
[14] H. Yang, H. Wang, G. F. Zou, M. Jain, N. A. Suvorova, D. M. Feldman, P. C. Dowden, R. F. DePaula, J. L. MacManus-Driscoll, A. J. Taylor, and Q. X. Jia, Appl. Phys. Lett. **93**, 142904 (2008).
[15] J. Wu, J. Wang, D. Xiao, and J. Zhu, Appl. Mater. Interfaces **3**, 2504 (2011).
[16] Y. W. Li, Z. G. Hu, F. Y. Yue, P. X. Yang, Y. N. Qian, W. J. Cheng, X. M. Ma, and J. H. Chu, J. Phys. D: Appl. Phys. **41**, 215403 (2008).
[17] S. J. Clark and J. Robertson, Appl. Phys. Lett. **90**, 132903 (2007).
[18] T. R. Paudel, S. J. Jaswal, and E. Y. Tsymbal, Phys. Rev. B **85**, 104409 (2012).
[19] Q. Xu, M. Sobhan, Q. Yang, F. Anariba, K. P. Ong, and P. Wy, Dalton Trans. **43**, 10787 (2014).
[20] A. J. Hauser, J. Zhang, L. Mier, R. A. Ricciardo, P. M. Woodward, T. L. Gustafson, L. J. Brillson, and F. Y. Yang, Appl. Phys. Lett. **92**, 222901 (2008).
[21] M. Yang, A. Bhatnagar, and M. Alexe, Adv. Electron. Mater. **1**, 1500139 (2015).
[22] K. Xiong and J. Robertson, Appl. Phys. Lett. **85**, 2577 (2004).
[23] C. H. Park and D. J. Chadi, Phys. Rev. Lett. **84**, 4717 (2000).
[24] R. V. Wang, D. D. Fong, F. Jiang, M. J. Highland, P. H. Fuoss, C. Thompson, A. M. Kolpak, J. A. Eastman, S. K. Streiffer, A. M. Rappe, and G. B. Stephenson, Phys. Rev. Lett. **102**, 047601 (2009).
[25] Y. Mi, G. Geneste, J. E. Rault, C. Mathieu, A. Pancotti, and N. Barrett, J. Phys.: Cond. Matt. **24**, 275901 (2012).
[26] T. Kolodiazhnyi, M. Tachibana, H. Kawaji, J. Hwang, and E. Takayama-Muromachi, Phys. Rev. Lett. **104**, 147602 (2010).
[27] Y. Wang, X. Liu, J. D. Burton, S. S. Jaswal, and E. Y. Tsymbal, Phys. Rev. Lett. **109**, 247601 (2012).

[28] L. He and D. Vanderbilt, Phys. Rev. B **68**, 134103 (2003).
[29] A. Chandrasekaran, D. Damjanovic, N. Setter, and N. Marzari, Phys. Rev. B **88**, 214116 (2013).
[30] C. Paillard, G. Geneste, L. Bellaiche, and B. Dkhil, J. Phys.: Cond. Matt. **29**, 485707 (2017).
[31] C.-H. Yang, D. Kan, I. Takeuchi, V. Nagarajan, and J. Seidel, Phys. Chem. Chem. Phys. **14**, 15953 (2012).
[32] J. H. Lee, J. H. Jeon, C. Yoon, S. Lee, Y. S. Kim, T. J. Oh, Y. H. Kim, J. Park, T. K. Song, and B. H. Park, Appl. Phys. Lett. **108**, 112902 (2016).
[33] T. You *et al.*, Sci. Rep. **5**, 18623 (2015).
[34] S. Lany and A. Zunger, Phys. Rev. B **78**, 235104 (2008).
[35] T. Tchelidze, T. Gagnidze, and A. Shengelaya, Phys. Status Solidi C **12**, 117 (2015).
[36] Y. Rui-Peng, L. Si-Xian, F. Xiao-Gong, Q. Ming-Hui, G. Xing-Sen, Z. Min, and L. Jun-Ming, Chin. Phys. B **23**, 067102 (2014).
[37] Z. Zhang, P. Wu, L. Chen, and J. Wang, Appl. Phys. Lett. **96**, 232906 (2010).
[38] C. Ederer and N. A. Spaldin, Phys. Rev. B **71**, 224103 (2005).
[39] S. J. Clark and J. Robertson, Appl. Phys. Lett. **94**, 022902 (2009).
[40] T. Shimada, T. Matsui, T. Xu, K. Arisue, Y. Zhang, J. Wang, and T. Kitamura, Phys. Rev. B **93**, 174107 (2016).
[41] J. B. Neaton, C. Ederer, U. V. Waghmare, N. A. Spaldin, and K. M. Rabe, Phys. Rev. B **71**, 014113 (2005).
[42] H. M. Tutuncu and G. P. Srivastava, J. Appl. Phys. **103**, 083712 (2008).
[43] D. Ricinschi, K.-Y. Yun, and M. Okuyama, J. Phys.: Cond. Matt. **18**, L97 (2006).
[44] P. Ravindran, R. Vidya, A. Kjekshus, H. Fjellvag, and O. Eriksson, Phys. Rev. B **74**, 224412 (2006).
[45] S. L. Shang, G. Sheng, Y. Wang, L. Q. Chen, and Z. K. Liu, Phys. Rev. B **80**, 052102 (2009).
[46] H. Wang, Y. Zheng, M.-Q. Cai, H. Huang, and H. L. W. Chan, Solid State Comm. **149**, 641 (2009).
[47] A. Stroppa and S. Picozzi, Phys. Chem. Chem. Phys. **12**, 5405 (2010).
[48] K. Knizek, Z. Jirak, J. Hejtmanek, P. Novak, and W. Ku, Phys. Rev. B **79**, 014430 (2009).
[49] H. Hsu, P. Blaha, and R. M. Wentzcovitch, Phys. Rev. B **85**, 140404(R) (2012).
[50] T. Jia, H. Wu, G. Zhang, X. Zhang, Y. Guo, Z. Zeng, and H.-Q. Lin, Phys. Rev. B **83**, 174433 (2011).
[51] H. Wu, J. Phys.: Cond. Matt. **15**, 503 (2003).
[52] W. Kohn and L. J. Sham, Phys. Rev. **140**, A1133 (1965).
[53] I. A. Kornev, S. Lisenkov, R. Haumont, B. Dkhil, and L. Bellaiche, Phys. Rev. Lett. **99**, 227602 (2007).
[54] J. P. Perdew, K. Burke, and M. Ernzerhof, Phys. Rev. Lett. **77**, 3865 (1996).
[55] X. Gonze *et al.*, Comput. Phys. Comm. **205**, 106 (2016).
[56] P. E. Blöchl, Phys. Rev. B **50**, 17953 (1994).
[57] M. Torrent, F. Jollet, F. Bottin, G. Zérah, and X. Gonze, Comput. Mat. Sci. **42**, 337 (2008).
[58] C. G. Van de Walle and A. Janotti, Advances in electronic structure methods for defects and impurities in solids, in *Advanced Calculations for Defects in Materials*, edited by A. Alkauskas, P. Deák, J. Neugebauer, A. Pasquarello, and C. G. Van de Walle (Wiley-VCH Verlag, Weinheim, Germany, 2011).
[59] G. Makov and M. C. Payne, Phys. Rev. B **51**, 4014 (1995).
[60] M. Graf, M. Sepliarsky, R. Machado, and M. G. Stachiotti, Solid State Commun. **218**, 10 (2015).
[61] S. Kamba, D. Nuzhnyy, M. Savinov, J. Sebek, J. Petzelt, J. Prokleska, R. Haumont, and J. Kreisel, Phys. Rev. B **75**, 024403 (2007).
[62] Y. Yao and H. Fu, Phys. Rev. B **84**, 064112 (2011).
[63] V. Kosyak, N. B. Mortazavi Amiri, A. V. Postnikov, M. A. Scarpulla, J. Appl. Phys. **114**, 124501 (2013).
[64] R. Vidya, P. Ravindran, H. Fjellvag, B. G. Svensson, E. Monakhov, M. Ganchenkova, and R. M. Nieminen, Phys. Rev. B **83**, 045206 (2011).
[65] P. Erhart, A. Klein, D. Aberg, and B. Sadigh, Phys. Rev. B **90**, 035204 (2014).
[66] A. Lindman, P. Erhart, and G. Wahnström, Phys. Rev. B **94**, 075204 (2016).
[67] H. Peng and S. Lany, Phys. Rev. B **85**, 201202(R) (2012).
[68] G. Jomard, B. Amadon, F. Bottin, and M. Torrent, Phys. Rev. B **78**, 075125 (2008).
[69] G. Geneste, B. Amadon, M. Torrent, and G. Dezanneau, Phys. Rev. B **96**, 134123 (2017).
[70] D. A. Freedman, D. Roundy, and T. A. Arias, Phys. Rev. B **80**, 064108 (2009).
[71] R. Nazarov, J. S. Majevadia, M. Patel, M. R. Wenman, D. S. Balint, J. Neugebauer, and A. P. Sutton, Phys. Rev. B **94**, 241112(R) (2016).
[72] E. Clouet, S. Garruchet, H. Nguyen, M. Perez, and C. S. Becquart, Acta Mater. **56**, 3450 (2008).
[73] C. Varvenne and E. Clouet, Phys. Rev. B **96**, 224103 (2017).
[74] A. N. Morozovska, E. A. Eliseev, M. D. Glinchuk, O. M. Fesenko, V. V. Shvartsman, V. Gopalan, M. V. Silibin, and D. V. Karpinsky, Phys. Rev. B **97**, 134115 (2018).
[75] F. Bruneval, C. Varvenne, J.-P. Crocombette, E. Clouet, Phys. Rev. B **91**, 024107 (2015).
[76] This is practically enforced with the ABINIT code by setting the variable *usedmatpu* to *-nstep*.
[77] M. Cococcioni and S. de Gironcoli, Phys. Rev. B **71**, 035105 (2005).